

STRUCTURED INVERSE-FREE NATURAL GRADIENT: MEMORY-EFFICIENT & NUMERICALLY-STABLE KFAC FOR LARGE NEURAL NETS

Wu Lin^{*,1} Felix Dangel^{*,1} Runa Eschenhagen³ Kirill Neklyudov¹
 Agustinus Kristiadi¹ Richard E. Turner³ Alireza Makhzani^{1,2}

¹Vector Institute ²University of Toronto ³University of Cambridge

ABSTRACT

Second-order methods for deep learning—such as KFAC—can be useful for neural net training. However, they are often memory-inefficient and numerically unstable for low-precision training since their preconditioning Kronecker factors are dense, and require high-precision matrix inversion or decomposition. Consequently, such methods are not widely used for training large neural networks such as transformer-based models. We address these two issues by (i) formulating an *inverse-free* update of KFAC and (ii) imposing *structures* in each of the Kronecker factors, resulting in a method we term *structured inverse-free natural gradient descent (SINGD)*. On large modern neural networks, we show that, in contrast to KFAC, SINGD is memory efficient and numerically robust, and often outperforms AdamW even in half precision. Hence, our work closes a gap between first-order and second-order methods in modern low precision training for large neural nets.

1 INTRODUCTION

The continuing success of deep learning (DL) is—to a large extent—powered by scaling up computational power (Thompson et al., 2020) to increase the number of neural network (NN) parameters that can be trained. Contemporary natural language processing (Radford et al., 2019; Brown et al., 2020; Touvron et al., 2023) and computer vision (Dehghani et al., 2023) models often consist of many billions of parameters, and will likely grow further in the future. To compensate for increasingly higher computational demands of training more parameters, many training pipelines use lower precision data types (Micikevicius et al., 2018) and memory-efficient first-order optimizers like SGD (Robbins & Monro, 1951) or Adam(W) (Kingma & Ba, 2015; Loshchilov & Hutter, 2019).

Second-order methods, like natural gradient descent (NGD, Amari, 1998), leverage curvature information which has many applications in deep learning: It is useful for improving training dynamics (Martens & Grosse, 2015; Osawa et al., 2023), pruning (Wang et al., 2019), understanding the influence of training examples (Bae et al., 2022), and uncertainty estimation (Zhang et al., 2018; Immer et al., 2021; Daxberger et al., 2021). One major obstacle why those methods are rarely used in deep learning is their higher memory consumption and iteration cost.

The perhaps most common concept to scale second-order methods for DL is Kronecker-factored approximate curvature (KFAC, Heskes, 2000; Martens & Grosse, 2015) which approximates the Fisher’s block diagonals via Kronecker products. While the KFAC optimizer, built on top of this curvature approximation, and its variants such as George et al. (2018) show promising results for medium-sized NNs (e.g. Osawa et al., 2023), their usefulness for large NN training is often limited by (i) memory consumption, and (ii) the use of low-precision floating-point (FP) training that renders matrix decompositions or inversions required to pre-condition the gradient numerically unstable.

Recently, Lin et al. (2023) proposed an inverse-free Kronecker-factored natural gradient descent (INGD) algorithm that replaces matrix inversion with subtraction in a matrix logarithm space. The algorithm’s update is purely based on matrix multiplications and therefore numerically stable in

^{*}Equal Contribution. Correspondence to: yorker.lin@gmail.com.

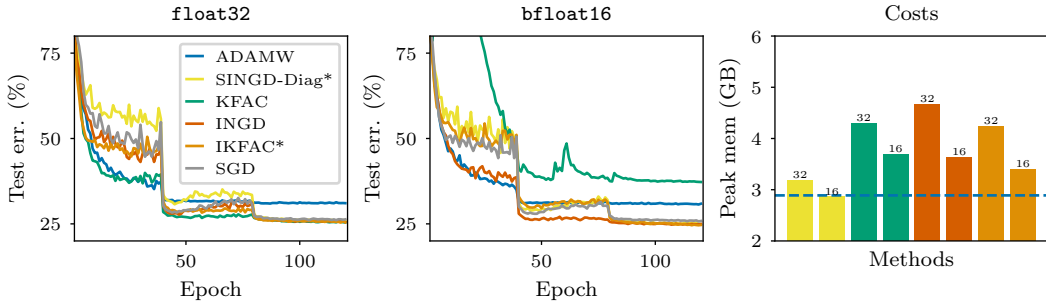


Figure 1: CIFAR-100 experiments on VGG net. *Left/Center*: Our methods (IKFAC and SINGD) outperform AdamW and perform stably in FP-32 and BFP-16—unlike KFAC—since they do not require matrix inversions/decompositions. IKFAC effectively performs KFAC updates and achieves similar performance in FP-32. For this task, replacing the dense Kronecker factors (INGD = SINGD-Dense) with diagonal ones (SINGD-Diag) does not harm performance while reducing computations. *Right*: Memory consumption of all methods. Removing Riemannian momentum (IKFAC) or using structured Kronecker factors (SINGD-Diag) reduces INGD’s memory consumption both in FP-32 and BFP-16. In BFP-16, SINGD-Diag achieves AdamW’s memory consumption (dashed line).

single-precision (FP-32); however, it is unclear whether this extends to half-precision (BFP-16). Furthermore, INGD has not been derived from the popular natural gradient approaches for DL. Hence, it is unclear if and how the method is connected to the predominant KFAC optimizer. Also, INGD does not improve over KFAC’s memory complexity since its Kronecker factors are dense matrices of the same size. And lastly, INGD has only been tested on convolution-based models and it is unclear whether it is useful for training modern transformer-based architectures (Vaswani et al., 2017).

Here, we extend INGD to lower its computational cost and theoretically resolve its connection to other approximate NGD methods for DL (see Figure 2 for an overview): First, we show that a special case of INGD recovers the KFAC method. This allows us to effectively perform KFAC updates in an *inverse-free* fashion. We call this modification of INGD *inverse-free KFAC (IKFAC)*. Second, we exploit an algebraic structure in the matrix logarithm space and propose structure-preserving updates to maintain sparse structures on Kronecker factors. This significantly reduces the memory cost and leads to a novel, scalable second-order optimization algorithm we call *structured inverse-free natural gradient descent (SINGD)* which contains INGD and IKFAC as special cases. We evaluate SINGD on convolution- and transformer-based models and show that it can (i) outperform SGD and AdamW while using as little memory as the latter thanks to structured Kronecker factors (see Table 3) and (ii) yield better performance than KFAC while being stable in half-precision. In summary:

- (a) We bridge the gap between INGD (Lin et al., 2023) and the original KFAC (Martens & Grosse, 2015), which requires matrix inversions that become unstable in low precision. Thereby, we effectively make KFAC inverse-free and amenable to low-precision training (Figure 1, left/center).
- (b) We impose various structures (block-diagonal, low-rank, Toeplitz, hierarchical) on the Kronecker factors of the INGD update, allowing them to be sparse to lower the memory consumption (Figure 1, right). We analyze the impact of a range of structures on downstream performance and find that sparse structures (see Fig. 5) that considerably lower the memory consumption (even lower than AdamW) can lead to competitive performance.
- (c) Unlike other second-order methods, we show that SINGD can stably train on a range of modern architectures (transformers, CNNs, GNNs) in BFloat16. Unlike first-order methods which are often useful in narrower scopes (SGD is best for CNNs, AdamW is best for transformers), SINGD works well and outperforms SGD and AdamW in many cases (see Sec. 4).

Our work closes a gap between first- and second-order methods in modern low precision training for large NNs. We release SINGD’s PyTorch implementation at github.com/f-dangel/singd.

2 PRELIMINARIES

We first introduce the necessary ingredients to establish a connection between INGD and KFAC, as they are derived from different perspectives. We start by describing Newton’s method as both methods can be seen as approximate Newton methods using NGD. Newton’s method is a classical second-order method to solve unconstrained optimization problems. NN training often corresponds to an unconstrained minimization problem. E.g., consider training a NN for image classification. Given a set of N examples $\{y_i, \mathbf{x}_i\}_{i=1}^N$ with labels y_i and images \mathbf{x}_i , the optimization problem is

$$\min_{\boldsymbol{\mu}} \ell(\boldsymbol{\mu}; \mathbf{y}, \mathbf{X}) := \min_{\boldsymbol{\mu}} \sum_{i=1}^N c(y_i, f(\boldsymbol{\mu}; \mathbf{x}_i)), \quad (1)$$

where $\mathbf{y} := (y_1, \dots, y_N)$, $\mathbf{X} := (\mathbf{x}_1, \dots, \mathbf{x}_N)$, and $\hat{y}_i := f(\boldsymbol{\mu}; \mathbf{x}_i)$ is a NN that outputs a predicted label \hat{y}_i for an image \mathbf{x}_i . Parameters $\boldsymbol{\mu}$ denote learnable weights of the NN, and $c(y_i, \hat{y}_i)$ is a differentiable loss function to measure the difference between a true label y_i and a predicted label \hat{y}_i . To solve Equation (1), Newton’s method follows the update

$$\boldsymbol{\mu} \leftarrow \boldsymbol{\mu} - \mathbf{S}^{-1} (\nabla_{\boldsymbol{\mu}} \ell(\boldsymbol{\mu}; \mathbf{y}, \mathbf{X})), \quad (2)$$

where $\mathbf{S} := \nabla_{\boldsymbol{\mu}}^2 \ell(\boldsymbol{\mu}; \mathbf{y}, \mathbf{X})$ is the Hessian of the loss.

2.1 KFAC: APPROXIMATE NGD FOR MAXIMUM LIKELIHOOD ESTIMATION

It is often computationally intractable to compute the Hessian of a NN model as required by Newton’s method. For natural gradient descent (Amari, 1998), a Fisher information matrix (FIM) is used instead of the Hessian matrix by reformulating problem (1) as maximum likelihood estimation (MLE) of a likelihood function $p(\mathbf{y}|\boldsymbol{\mu}, \mathbf{X}) = \prod_i p(y_i|\boldsymbol{\mu}, \mathbf{x}_i)$, where $p(y_i|\boldsymbol{\mu}, \mathbf{x}_i) := \exp(-c(y_i, f(\boldsymbol{\mu}, \mathbf{x}_i)))$. In this case, the minimization problem is equivalent to the MLE problem:

$$\max_{\boldsymbol{\mu}} p(\mathbf{y}|\boldsymbol{\mu}, \mathbf{X}) \iff \min_{\boldsymbol{\mu}} -\log p(\mathbf{y}|\boldsymbol{\mu}, \mathbf{X}) = \min_{\boldsymbol{\mu}} \ell(\boldsymbol{\mu}; \mathbf{y}, \mathbf{X}). \quad (3)$$

The MLE problem formulation allows us to exploit additional statistical structures such as the FIM. The FIM for the MLE problem is defined as shown below (Kunstner et al., 2019), where we assume a label y is sampled from the distribution $p(y|\boldsymbol{\mu}, \mathbf{x}_i)$ given an image \mathbf{x}_i :

$$F(\boldsymbol{\mu}) := \sum_{i=1}^N \mathbb{E}_{y \sim p(y|\boldsymbol{\mu}, \mathbf{x}_i)} [\nabla_{\boldsymbol{\mu}} \log p(y|\boldsymbol{\mu}, \mathbf{x}_i) \nabla_{\boldsymbol{\mu}}^T \log p(y|\boldsymbol{\mu}, \mathbf{x}_i)] = \sum_{i=1}^N \mathbb{E}_{y \sim p(y|\boldsymbol{\mu}, \mathbf{x}_i)} [-\nabla_{\boldsymbol{\mu}}^2 \log p(y|\boldsymbol{\mu}, \mathbf{x}_i)]. \quad (4)$$

For ubiquitous loss functions like the mean-squared error and cross-entropy, and more generally, many members of the exponential family with natural parameterization, the FIM coincides with the generalized Gauss-Newton (GGN) matrix (Wang, 2010; Martens, 2014), a common approximation of the Hessian in deep learning (Schaudolph, 2002; Botev et al., 2017). This relationship connects NGD to Newton’s method. A common approximation of the FIM/GGN and Hessian is the so-called *empirical Fisher* $\hat{F}(\boldsymbol{\mu})$, which replaces the samples y from the model’s predictive distribution in Eq. (4) with the empirical labels y_i from the data:

$$\hat{F}(\boldsymbol{\mu}) := \sum_{i=1}^N \nabla_{\boldsymbol{\mu}} \log p(y_i|\boldsymbol{\mu}, \mathbf{x}_i) \nabla_{\boldsymbol{\mu}}^T \log p(y_i|\boldsymbol{\mu}, \mathbf{x}_i) \approx -\sum_{i=1}^N \nabla_{\boldsymbol{\mu}}^2 \log p(y_i|\boldsymbol{\mu}, \mathbf{x}_i) = \mathbf{S}.$$

While there is no clear theoretical justification for this approximation of the Hessian (Kunstner et al., 2019), it simplifies the implementation and reduces the cost, and has been shown to work well in practice (Graves, 2011; Osawa et al., 2019). This approximation is also known as Fisher’s scoring with observed FIM for nonlinear models (Osborne, 1992; Smyth, 1996; 2015). With this, we can formulate an NGD update with the *empirical* FIM $\hat{F}(\boldsymbol{\mu})$ to approximate Newton’s method as

$$\boldsymbol{\mu} \leftarrow \boldsymbol{\mu} - \beta \left(\hat{F}(\boldsymbol{\mu}) \right)^{-1} \nabla_{\boldsymbol{\mu}} \ell(\boldsymbol{\mu}; \mathbf{y}, \mathbf{X}) \approx \boldsymbol{\mu} - \beta \mathbf{S}^{-1} \nabla_{\boldsymbol{\mu}} \ell(\boldsymbol{\mu}; \mathbf{y}, \mathbf{X}).$$

We call this update NGD for MLE.

Kronecker-Factored Approximate Curvature (Heskes, 2000; Martens & Grosse, 2015, KFAC) is the probably most commonly used second-order optimizer in deep learning. The KFAC algorithm is based on a Kronecker-factored approximation of the Fisher, which is also sometimes referred to as KFAC. Here, we refer to the algorithm as *KFAC* or *KFAC method* and to the approximation as *Kronecker approximation*. In this work, we consider the Kronecker approximation of the *empirical*

Fisher. The Kronecker approximation of the Fisher approximates the FIM with a block-diagonal matrix, where each block F_l is a Kronecker-factored matrix and corresponds to layer l of the neural network. This approximation has first been derived for linear layers, later for convolutional (Grosse & Martens, 2016) and recurrent layers (Martens et al., 2018), and has recently been generalized to all linear layers that use weight sharing (Eschenhagen et al., 2023), e.g. also graph neural networks and transformers. The blocks are defined as $\tilde{F}_l(\boldsymbol{\mu}) := \mathbf{U}_l \otimes \mathbf{G}_l$, where $\mathbf{U}_l := \mathbf{u}_l \mathbf{u}_l^\top \in \mathbb{R}^{d_i \times d_i}$ and $\mathbf{G}_l := \mathbf{g}_l \mathbf{g}_l^\top \in \mathbb{R}^{d_o \times d_o}$. The vector $\mathbf{u}_l \in \mathbb{R}^{d_i}$ is the input to the l th layer and $\mathbf{g}_l \in \mathbb{R}^{d_o}$ is the gradient of the loss ℓ w.r.t. the output of the l th layer. We have suppressed the dependence on the parameters $\boldsymbol{\mu}$ and the input \mathbf{x}_i and assume that there is no weight sharing for simplicity. The KFAC method uses exponential moving averages (β_1) over \mathbf{U} and \mathbf{G} , yielding \mathbf{S}_K , \mathbf{S}_C , and damping λ , see Fig. 3.

While the Kronecker approximation allows for much more efficient preconditioning of the gradient, the dense Kronecker factors \mathbf{S}_K and \mathbf{S}_C still have to be stored and inverted at every preconditioner update when using the KFAC method. While the computational overhead can usually be amortized by updating the preconditioner less frequently, this can lead to (i) numerical instability, especially in low-precision settings, and (ii) memory issues for large models. Since low-precision training of large models is becoming the norm in fields like natural language processing, these issues will become more apparent in modern deep learning. There are multiple numerical concerns when using the KFAC method or its variants such as George et al. (2018) in the low precision setting. In PyTorch (Paszke et al., 2019) and Jax (Bradbury et al., 2018) implementations, all tensors have to be transformed into 32 bit floats since there is no support for 16 bit matrix inverse or decomposition operations. Moreover, over- or underflow can be an issue when calculating \mathbf{G}_l and the gradient \mathbf{g}_l has to be rescaled to improve stability. Memory constraints have previously been addressed by using a diagonal or block-diagonal approximation to the Kronecker factors (Zhang et al., 2018; Grosse et al., 2023). However, it is unclear if downstream performance can be maintained by using these simple structures.

2.2 INGD: APPROXIMATE NGD FOR BAYESIAN PARAMETER ESTIMATION

Derived from Bayesian principles, the INGD method (Lin et al., 2023) directly approximates the inverse of the Hessian. We first introduce the Bayesian learning rule (BLR, Khan & Lin, 2017; Zhang et al., 2018; Khan et al., 2018; Osawa et al., 2019; Lin et al., 2020; Khan & Rue, 2021; Tan, 2022) and an inverse-free second-order method (Lin et al., 2021) as the INGD method builds on these works.

By the BLR, Newton’s method to solve the MLE problem in (3) can be interpreted as another natural-gradient update to solve a variational inference problem (5) with a delta approximation (Khan & Rue, 2021). This interpretation allows us to view a precision matrix in the variational problem as Hessian estimation in the MLE problem. Thus, Lin et al. (2021) suggest reparameterizing the Hessian as the precision of the Gaussian posterior in a matrix logarithm space and exploiting the parameterization invariance of natural-gradients to obtain an inverse-free update scheme.

We now describe the learning rule and relate the natural gradient update to Newton’s method. We consider a Bayesian problem formulation, where NN weights are random variables. We denote these weights by new parameters \mathbf{w} since random variables are no longer learnable. We use a variational Gaussian distribution to approximate the posterior distribution of the random variables. Later on, we will show that the natural-gradient update of the Gaussian distribution recovers Newton’s method for the learnable parameters. The mean and the precision matrix of the Gaussian will be treated as the learnable weights $\boldsymbol{\mu}$ and the Hessian estimation \mathbf{S} in Newton’s step (see (2)), respectively.

The variational inference problem considered in the learning rule is defined as

$$\min_{\boldsymbol{\tau}} -\mathcal{L}(\boldsymbol{\tau}) := \mathbb{E}_{\mathbf{w} \sim q(\mathbf{w}; \boldsymbol{\tau})} [-\log p(\mathbf{w}) - \log p(\mathbf{y}|\mathbf{w}, \mathbf{X})] - H_q(\boldsymbol{\tau}), \quad (5)$$

where $\mathcal{L}(\boldsymbol{\tau})$ is known as the evidence lower bound (ELBO), $\boldsymbol{\tau} = \{\boldsymbol{\mu}, \mathbf{S}\}$ are the learnable parameters of the variational distribution $q(\mathbf{w}|\boldsymbol{\tau}) = \mathcal{N}(\mathbf{w}|\boldsymbol{\mu}, \mathbf{S})$ which is a Gaussian distribution with mean $\boldsymbol{\mu}$ and precision \mathbf{S} . The likelihood $p(\mathbf{y}|\mathbf{w}, \mathbf{X}) = \exp(-\ell(\mathbf{w}; \mathbf{y}, \mathbf{X}))$ takes the same form considered in the MLE setting while the prior $p(\mathbf{w}) \propto \exp(-R(\mathbf{w}))$ is defined by a regularizer $R(\mathbf{w}) \geq 0$. To recover the MLE problem, we consider an uninformative prior $p(\mathbf{w})$ (i.e., $R(\mathbf{w}) = 0$). Finally, the function $H_q(\boldsymbol{\tau}) := \mathbb{E}_{\mathbf{w} \sim q} [-\log q]$ is the entropy of distribution $q(\mathbf{w}; \boldsymbol{\tau})$.

Similar to the MLE case, the Bayesian problem formulation also allows us to exploit additional statistical structures such as another FIM. The FIM used in the BLR is the FIM of the variational

Gaussian distribution defined as

$$F(\boldsymbol{\tau}) := \mathbb{E}_{w \sim q(w|\boldsymbol{\tau})} [\nabla_{\boldsymbol{\tau}} \log q(\mathbf{w}|\boldsymbol{\tau}) \nabla_{\boldsymbol{\tau}}^T \log q(\mathbf{w}|\boldsymbol{\tau})],$$

which has a closed-form expression and should not be confused with the FIM used for MLE (4).

Under the BLR, we perform NGD updates not only on $\boldsymbol{\mu}$ but also on \mathbf{S} . A NGD step (Khan & Rue, 2021) with the *exact* FIM $F(\boldsymbol{\tau})$ and stepsize $\beta > 0$ to update $\boldsymbol{\tau} = \{\boldsymbol{\mu}, \mathbf{S}\}$ is defined as

$$\boldsymbol{\tau} \leftarrow \boldsymbol{\tau} - \beta \left(F(\boldsymbol{\tau}) \right)^{-1} \nabla_{\boldsymbol{\tau}} (-\mathcal{L}(\boldsymbol{\tau})).$$

This is the NGD update for BLR, vis-à-vis for MLE. We can simplify the update (Khan et al., 2018):

$$\mathbf{S} \leftarrow (1 - \beta) \mathbf{S} + \beta \mathbb{E}_{w \sim q(w;\boldsymbol{\mu}, \mathbf{S})} [\nabla_w^2 \ell(\mathbf{w}; \mathbf{y}, \mathbf{X})], \quad \boldsymbol{\mu} \leftarrow \boldsymbol{\mu} - \beta \mathbf{S}^{-1} \mathbb{E}_{w \sim q(w;\boldsymbol{\mu}, \mathbf{S})} [\nabla_w \ell(\mathbf{w}; \mathbf{y}, \mathbf{X})].$$

Then, to recover Newton's method in (2), we approximate the update rule above with

$$\mathbf{S} \leftarrow (1 - \beta) \mathbf{S} + \beta \nabla_{\boldsymbol{\mu}}^2 \ell(\boldsymbol{\mu}; \mathbf{y}, \mathbf{X}), \quad \boldsymbol{\mu} \leftarrow \boldsymbol{\mu} - \beta \mathbf{S}^{-1} \nabla_{\boldsymbol{\mu}} \ell(\boldsymbol{\mu}; \mathbf{y}, \mathbf{X}),$$

by (i) using a delta approximation at mean $\boldsymbol{\mu}$ to approximate expectations highlighted in red and (ii) setting the stepsize β to 1.

Lin et al. (2021) suggest reparameterizing the precision matrix \mathbf{S} in a matrix logarithm space and performing natural-gradient updates in this space. By performing NGD in the logarithm space, we can transform matrix inversion into matrix subtraction. We then go back directly to the space of the matrix inverse without explicitly inverting any matrix by using a truncated matrix exponential. Thus, the method is inverse-free and Newton-like since the natural-gradient update is parameterization invariant and resembles Newton's step by rephrasing the update in terms of \mathbf{S} .

We now describe the inverse-free method. We first re-express the precision matrix \mathbf{S} using a non-singular square matrix \mathbf{A} as $\mathbf{S} = \mathbf{A}^{-T} \mathbf{A}^{-1}$ and perform a natural-gradient step using the exact FIM in a tangent space (denoted by \mathbf{M}) of \mathbf{A}_t at iteration t . We then construct a new map as $\mathbf{A} := \phi(\mathbf{A}_t, \mathbf{M}) := \mathbf{A}_t \text{Expm}(1/2\mathbf{M})$ using both the current point \mathbf{A}_t and parameter \mathbf{M} as input, where $\text{Expm}(\mathbf{N}) = \mathbf{I} + \sum_{j=1}^{\infty} \mathbf{N}^j / j!$ is the matrix exponential. Observe that \mathbf{M} stays in a matrix logarithm space. At each iteration k , we use a new matrix logarithm space associated to \mathbf{A}_k and generate a new origin $\mathbf{M}_0 = \mathbf{0}$ in this space to represent \mathbf{A}_k since $\mathbf{A}_k \equiv \phi(\mathbf{A}_k, \mathbf{M}_0) = \mathbf{A}_k \text{Expm}(1/2\mathbf{M}_0)$. The map ϕ is a *local reparameterization* map as it takes not only \mathbf{M} but also \mathbf{A}_k as input. Thanks to this map, the Fisher block is *locally orthonormalized* (Lin et al., 2023) at origin \mathbf{M}_0 . Thus, a natural-gradient step becomes a (Euclidean) gradient step, which makes it easy to add Riemannian momentum into the structured positive-definite matrix \mathbf{S} (Lin et al., 2023). Importantly, this map allows us to perform updates in the space of \mathbf{M} as the matrix logarithm space to avoid performing matrix inversions:

$$\mathbf{M} \leftarrow \mathbf{M}_0 - \beta \mathbf{N}, \quad \boldsymbol{\mu} \leftarrow \boldsymbol{\mu} - \beta \mathbf{A}_{t+1} \mathbf{A}_{t+1}^T \nabla_{\boldsymbol{\mu}} \ell(\boldsymbol{\mu}; \mathbf{y}, \mathbf{X}), \quad (6)$$

where $\mathbf{N} := \mathbf{A}_t^T \nabla_{\boldsymbol{\mu}}^2 \ell(\boldsymbol{\mu}; \mathbf{y}, \mathbf{X}) \mathbf{A}_t - \mathbf{I}$ and $\mathbf{A}_{t+1} := \phi(\mathbf{A}_t, \mathbf{M}) = \mathbf{A}_t \text{Expm}(1/2\mathbf{M})$.

The above update is a Newton-like update without matrix inverse. To see that, we can reexpress the update of \mathbf{A} in terms of \mathbf{S} :

$$\mathbf{S}_{t+1} = \mathbf{A}_{t+1}^{-T} \mathbf{A}_{t+1}^{-1} = \mathbf{A}_t^{-T} \text{Expm}(\beta \mathbf{N}) \mathbf{A}_t^{-1} = (1 - \beta) \mathbf{S}_t + \beta \nabla_{\boldsymbol{\mu}}^2 \ell(\boldsymbol{\mu}; \mathbf{y}, \mathbf{X}) + O(\beta^2), \quad (7)$$

using the properties of the matrix exponential function.

It is essential to update \mathbf{M} to preserve sparsity in \mathbf{A} as we will discuss this point in Sec. 3.2. The space of \mathbf{M} as a tangent/logarithm space of \mathbf{A} allows us to impose sparse structures on \mathbf{A} without requiring the Hessian $\nabla_{\boldsymbol{\mu}}^2 \ell(\boldsymbol{\mu}; \mathbf{y}, \mathbf{X})$ or a Hessian approximation to be sparse or structured. Another inverse-free method (Tan, 2022) considers directly performing NGD updates of \mathbf{A} instead of \mathbf{M} , where \mathbf{A} must be restricted to a (triangular) Cholesky factor. However, the approach of Tan (2022) does not preserve sparsity in \mathbf{A} unless the Hessian or the approximation admits a special model-specific structure. For many deep learning problems, the Hessian or the approximation does not have such a special structure. Thus, we consider the approach of Lin et al. (2021) to impose sparsity on \mathbf{A} .

Our work is built on the INGD method (summarized in Fig. 4) where $\mathbf{A} = \mathbf{K} \otimes \mathbf{C}$ is factorized by two Kronecker factors. The exact FIM under this parameterization is singular due to a correlation between

\mathbf{K} and \mathbf{C} . This is because the Kronecker factorization is not unique. We can use a (non-singular) block-diagonal approximated FIM by ignoring the correlation in the original FIM. Lin et al. (2023) suggest performing NGD with this block-diagonal FIM on tangent spaces of the factors instead. Riemannian momentum is further introduced in the update of \mathbf{K} and \mathbf{C} . The authors suggest using the Kronecker approximation discussed in Section 2.1 to approximate the Hessian $\nabla_{\mu}^2 \ell(\mu; \mathbf{y}, \mathbf{X})$ and truncating the matrix exponential to obtain a purely matrix-multiplication based update scheme. However, it is unclear how the proposed update is related to the KFAC update (summarized in Fig. 3) where another Kronecker factorization such as $\mathbf{S} = \mathbf{S}_K \otimes \mathbf{S}_C$ is used. Moreover, the INGD method remains memory inefficient for large neural networks due to the use of dense Kronecker factors. Last but not least, the authors only consider and evaluate the update on convolution-based models using single floating-point precision. It remains unclear whether the proposed update can be applicable in modern settings such as training transformer-based models and using half-precision for training.

3 OUR CONTRIBUTION: STRUCTURED INVERSE-FREE NGD

Inspired by the INGD method, we propose an inverse-free KFAC update scheme as a specific setting of the INGD method to address the numerical instability of the KFAC method for low-precision training. We show that this scheme effectively recovers the KFAC method. We then address the memory inefficiency of the KFAC and the INGD method for training large NNs such as transformer-based models by extending the INGD method.

3.1 INVERSE-FREE KFAC UPDATES FOR IMPROVING NUMERICAL STABILITY

We first propose a new inverse-free update scheme to mimic the behavior of the KFAC update. We refer to this update as IKFAC or the IKFAC update. We then show that IKFAC corresponds to a specific setting of the INGD method. Thus, our approach bridges the gap between INGD and KFAC, and sheds light on the difference between both methods. Our approach also makes it easy to switch from the INGD update to the KFAC update while keeping updates numerically stable.

Inspired by the INGD method, we replace matrix inversion with matrix subtraction in a matrix logarithm space and use a truncated matrix exponential map to go back to the space of the inverse matrix without explicitly inverting any matrix. The IKFAC update is related to the KFAC update as we will use $\mathbf{K}\mathbf{K}^{\top}$ and $\mathbf{C}\mathbf{C}^{\top}$ to approximate the inverse Kronecker factors $(\mathbf{S}_K + \lambda\mathbf{I})^{-1}$ and $(\mathbf{S}_C + \lambda\mathbf{I})^{-1}$ in the KFAC update, respectively. We propose the following IKFAC update with learning rate β_1 for \mathbf{K} and \mathbf{C} using a truncated matrix exponential¹

$$\mathbf{K}^{\text{new}} \leftarrow \mathbf{K} \left(\mathbf{I} - \frac{\beta_1}{2} \mathbf{m}_K \right), \quad \mathbf{C}^{\text{new}} \leftarrow \mathbf{C} \left(\mathbf{I} - \frac{\beta_1}{2} \mathbf{m}_C \right), \quad (8)$$

where $\mathbf{H}_K := \mathbf{K}^{\top} \mathbf{U} \mathbf{K}$, $\mathbf{H}_C := \mathbf{C}^{\top} \mathbf{G} \mathbf{C}$, $\mathbf{m}_K := \mathbf{H}_K + \lambda \mathbf{K}^{\top} \mathbf{K} - \mathbf{I}$, $\mathbf{m}_C := \mathbf{H}_C + \lambda \mathbf{C}^{\top} \mathbf{C} - \mathbf{I}$.

Observe that the IKFAC update in (8) is inverse-free and matrix-decomposition-free. As shown in Appendix D, \mathbf{m}_K indeed stays in a matrix logarithm space since we use the truncated matrix exponential $\text{Expm}(-\frac{\beta_1}{2} \mathbf{m}_K) \approx (\mathbf{I} - \beta_1/2 \mathbf{m}_K)$ in the update (see (8)). The logarithm space allows us to impose structural constraints on \mathbf{K} as we will discuss them in the next section.

The following theorem—proof in Appendix E—formally shows that $\mathbf{K}\mathbf{K}^{\top}$ used in the IKFAC update is an approximation of $(\mathbf{S}_K + \lambda\mathbf{I})^{-1}$ in the KFAC update at every step even when the truncated matrix exponential is employed. Similarly, we can show $\mathbf{C}\mathbf{C}^{\top}$ is an approximation of $(\mathbf{S}_C + \lambda\mathbf{I})^{-1}$. Thus, the IKFAC update effectively recovers the KFAC update up to a first-order accuracy.

Theorem 1 *If the update of \mathbf{K} is updated according to the IKFAC update scheme (see Fig. 3) with the truncation of the matrix exponential and these two updates use the same initialization and the same sequence of curvature matrices \mathbf{U} , then the product $\mathbf{K}\mathbf{K}^{\top}$ has a first-order accuracy of the KFAC update of $(\mathbf{S}_K + \lambda\mathbf{I})^{-1}$ at each iteration, i.e., $\mathbf{K}\mathbf{K}^{\top} = (\mathbf{S}_K + \lambda\mathbf{I})^{-1} + O(\beta_1^2)$.*

¹ \mathbf{K} and \mathbf{C} could be singular if using this first-order truncation. They can be non-singular if we use a second-order truncation of the exponential. Nevertheless, the first-order truncation works very well in practice.

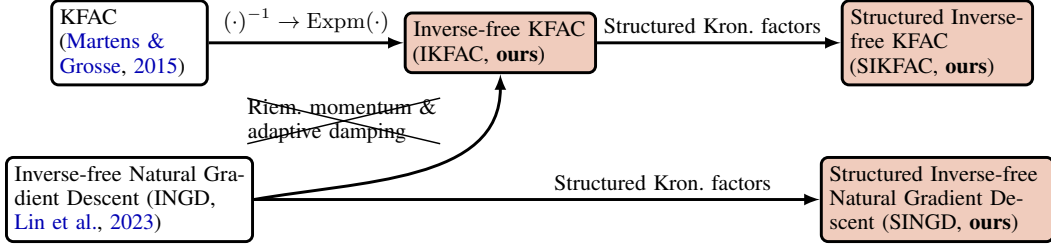


Figure 2: Overview of existing methods and their relation to our proposed methods. IKFAC behaves like KFAC (Theorem 1), but is numerically stable in lower precision. In contrast to IKFAC, INGD has Riemannian momenta, and adaptive damping and curvature which could lead to better performance in practice (Section 4). INGD is equivalent to SINGD with unstructured Kronecker factors (SINGD-Dense). Structured Kronecker factors reduce memory consumption and computational cost.

KFAC (Martens & Grosse, 2015)

- 1: Each T iters, update $\mathbf{s}_K, \mathbf{s}_C$
Obtain $\mathbf{U} \otimes \mathbf{G}$ to approximate $\nabla_\mu^2 \ell(\boldsymbol{\mu})$
 $\mathbf{s}_K \leftarrow (1 - \beta_1) \mathbf{s}_K + \beta_1 \mathbf{U}$
 $\mathbf{s}_C \leftarrow (1 - \beta_1) \mathbf{s}_C + \beta_1 \mathbf{G}$
 $\mathbf{s}_K^{-1} \leftarrow (\mathbf{s}_K + \lambda \mathbf{I}_{d_i})^{-1}$
 $\mathbf{s}_C^{-1} \leftarrow (\mathbf{s}_C + \lambda \mathbf{I}_{d_o})^{-1}$
- 2: $\mathbf{m}_\mu \leftarrow \alpha_2 \mathbf{m}_\mu + \mathbf{s}_C^{-1} \text{vec}^{-1}(\mathbf{g}) \mathbf{s}_K^{-1} + \gamma \text{vec}^{-1}(\boldsymbol{\mu})$
- 3: $\boldsymbol{\mu} \leftarrow \boldsymbol{\mu} - \beta_2 \text{vec}(\mathbf{m}_\mu)$

IKFAC (ours)

- 1: Each T iters, update $\mathbf{m}_K, \mathbf{m}_C, \mathbf{K}, \mathbf{C}$
Obtain $\mathbf{U} \otimes \mathbf{G}$ to approximate $\nabla_\mu^2 \ell(\boldsymbol{\mu})$
 $\mathbf{m}_K \leftarrow \mathbf{0} \mathbf{m}_K + \frac{1}{2d_o} (\mathbf{d}_o \mathbf{H}_K + \lambda \mathbf{d}_o \mathbf{K}^\top \mathbf{K} - \mathbf{d}_o \mathbf{I}_{d_i})$
 $\mathbf{m}_C \leftarrow \mathbf{0} \mathbf{m}_C + \frac{1}{2d_i} (\mathbf{d}_i \mathbf{H}_C + \lambda \mathbf{d}_i \mathbf{C}^\top \mathbf{C} - \mathbf{d}_i \mathbf{I}_{d_o})$
 $\mathbf{K} \leftarrow \mathbf{K} (\mathbf{I}_{d_i} - \beta_1 \mathbf{m}_K)$
 $\mathbf{C} \leftarrow \mathbf{C} (\mathbf{I}_{d_o} - \beta_1 \mathbf{m}_C)$
- 2: $\mathbf{m}_\mu \leftarrow \alpha_2 \mathbf{m}_\mu + \mathbf{C} \mathbf{C}^\top \text{vec}^{-1}(\mathbf{g}) \mathbf{K} \mathbf{K}^\top + \gamma \text{vec}^{-1}(\boldsymbol{\mu})$
- 3: $\boldsymbol{\mu} \leftarrow \boldsymbol{\mu} - \beta_2 \text{vec}(\mathbf{m}_\mu)$

Figure 3: Comparison between KFAC and IKFAC update for one weight matrix $\text{vec}^{-1}(\boldsymbol{\mu}) \in \mathbb{R}^{d_o \times d_i}$. The flattened gradient is $\mathbf{g} := \nabla_\mu \ell(\boldsymbol{\mu}) \in \mathbb{R}^{d_o d_i}$ and $\text{vec}^{-1}(\mathbf{g}) \in \mathbb{R}^{d_o \times d_i}$ is its matrix reshape. IKFAC uses $\mathbf{H}_K := \mathbf{K}^\top \mathbf{U} \mathbf{K}$ and $\mathbf{H}_C := \mathbf{C}^\top \mathbf{G} \mathbf{C}$ to incorporate the Kronecker curvature \mathbf{U} and \mathbf{G} . Both methods use momentum buffers \mathbf{m}_μ for the weight-decayed update direction with momentum α_2 and weight decay γ , and a learning rate β_2 for the parameter update. (Left) KFAC uses an exponentially moving average with decay $1 - \beta_1$ to accumulate the Kronecker factors and applies a damping term $\lambda \mathbf{I}$ before inversion to handle potential singularities in $\mathbf{s}_K, \mathbf{s}_C$. (Right) In contrast to KFAC, IKFAC directly approximates $(\mathbf{s}_K + \lambda \mathbf{I})^{-1}$ and $(\mathbf{s}_C + \lambda \mathbf{I})^{-1}$ by $\mathbf{K} \mathbf{K}^\top$ and $\mathbf{C} \mathbf{C}^\top$. The pre-conditioner update is a modification of INGD (Lin et al., 2023) and the changes—zero Riemannian momentum, and non-adaptive damping and curvature—are highlighted in red.

INGD (Lin et al., 2023)

- 1: Each T iterations, update $\mathbf{m}_K, \mathbf{m}_C, \mathbf{K}, \mathbf{C}$
Obtain $\mathbf{U} \otimes \mathbf{G}$ to approximate $\nabla_\mu^2 \ell(\boldsymbol{\mu})$
 $\mathbf{m}_K \leftarrow \alpha_1 \mathbf{m}_K + \frac{1}{2d_o} (\text{Tr}(\mathbf{H}_C) \mathbf{H}_K + c^2 \mathbf{K}^\top \mathbf{K} - d_o \mathbf{I}_{d_i})$
 $\mathbf{m}_C \leftarrow \alpha_1 \mathbf{m}_C + \frac{1}{2d_i} (\text{Tr}(\mathbf{H}_K) \mathbf{H}_C + \kappa^2 \mathbf{C}^\top \mathbf{C} - d_i \mathbf{I}_{d_o})$
 $\mathbf{K} \leftarrow \mathbf{K} (\mathbf{I}_{d_i} - \beta_1 \mathbf{m}_K)$
 $\mathbf{C} \leftarrow \mathbf{C} (\mathbf{I}_{d_o} - \beta_1 \mathbf{m}_C)$
- 2: $\mathbf{m}_\mu \leftarrow \alpha_2 \mathbf{m}_\mu + \mathbf{C} \mathbf{C}^\top \text{vec}^{-1}(\mathbf{g}) \mathbf{K} \mathbf{K}^\top + \gamma \text{vec}^{-1}(\boldsymbol{\mu})$
- 3: $\boldsymbol{\mu} \leftarrow \boldsymbol{\mu} - \beta_2 \text{vec}(\mathbf{m}_\mu)$

SINGD (ours)

- 1: Each T iterations, update $\hat{\mathbf{L}} \mathbf{m}_K, \hat{\mathbf{L}} \mathbf{m}_C, \hat{\mathbf{L}} \mathbf{K}, \hat{\mathbf{L}} \mathbf{C}$
Obtain $\mathbf{U} \otimes \mathbf{G}$ to approximate $\nabla_\mu^2 \ell(\boldsymbol{\mu})$
 $\hat{\mathbf{L}} \mathbf{m}_K \leftarrow \alpha_1 \hat{\mathbf{L}} \mathbf{m}_K + \frac{1}{2d_o} \hat{\Pi}_K (\text{Tr}(\mathbf{H}_{\mathcal{L}_C}) \mathbf{H}_{\mathcal{L}_K} + c^2 (\hat{\mathbf{L}} \mathbf{K})^\top \hat{\mathbf{L}} \mathbf{K} - d_o \mathbf{I}_{d_i})$
 $\hat{\mathbf{L}} \mathbf{m}_C \leftarrow \alpha_1 \hat{\mathbf{L}} \mathbf{m}_C + \frac{1}{2d_i} \hat{\Pi}_C (\text{Tr}(\mathbf{H}_{\mathcal{L}_K}) \mathbf{H}_{\mathcal{L}_C} + \kappa^2 (\hat{\mathbf{L}} \mathbf{C})^\top \hat{\mathbf{L}} \mathbf{C} - d_i \mathbf{I}_{d_o})$
 $\hat{\mathbf{L}} \mathbf{K} \leftarrow \hat{\mathbf{L}} \mathbf{K} (\mathbf{I}_{d_i} - \beta_1 \hat{\mathbf{L}} \mathbf{m}_K)$
 $\hat{\mathbf{L}} \mathbf{C} \leftarrow \hat{\mathbf{L}} \mathbf{C} (\mathbf{I}_{d_o} - \beta_1 \hat{\mathbf{L}} \mathbf{m}_C)$
- 2: $\mathbf{m}_\mu \leftarrow \alpha_2 \mathbf{m}_\mu + \hat{\mathbf{L}} \mathbf{C} (\hat{\mathbf{L}} \mathbf{C})^\top \text{vec}^{-1}(\mathbf{g}) \hat{\mathbf{L}} \mathbf{K} (\hat{\mathbf{L}} \mathbf{K})^\top + \gamma \text{vec}^{-1}(\boldsymbol{\mu})$
- 3: $\boldsymbol{\mu} \leftarrow \boldsymbol{\mu} - \beta_2 \text{vec}(\mathbf{m}_\mu)$

Figure 4: Comparison of a single weight matrix’s update between INGD and our extension—SINGD—via structured Kronecker factors. (Left) INGD features **Riemannian momentum** (α_1), **adaptive curvature** ($\text{Tr}(\mathbf{H}_C)$, $\text{Tr}(\mathbf{H}_K)$), **adaptive damping** ($c^2 := \lambda \text{Tr}(\mathbf{C}^\top \mathbf{C})$, $\kappa^2 := \lambda \text{Tr}(\mathbf{K}^\top \mathbf{K})$), and **correlated updates** of \mathbf{K} and \mathbf{C} ($\mathbf{m}_K, \mathbf{m}_C$). The pre-conditioner matrices are updated with a learning rate β_1 , and the optimizer keeps a momentum buffer on the weight-decayed update with momentum α_2 and weight decay γ . The learning rate to update the parameters is β_2 . (Right) SINGD’s update is similar but each Kronecker factor and its momentum (•) is replaced by its **structured version** ($\hat{\mathbf{L}} \bullet$, e.g. (block-)diagonal); likewise in the computation of $c^2, \kappa^2, \mathbf{H}_K$, and \mathbf{H}_C . When updating the momenta, their structure is preserved through a **subspace projection map** $\hat{\Pi}_\bullet(\cdot)$ that restores $\hat{\mathbf{L}} \bullet$ ’s structure from a dense symmetric matrix \cdot (e.g. taking the (block) diagonal). Importantly, we can efficiently compute the extraction map without expanding its argument in dense form, which reduces memory and run time. The extension of INGD and SINGD is analogous. One of the notable elements of INGD and SINGD is that they are scale invariant to the choice of the Kronecker approximation (see Appx. F) as the approximation is not unique. In contrast, KFAC and IKFAC are not scale invariant to the approximation.

Now, we show that the IKFAC scheme is a specific setting of the INGD method. As shown in Fig. 4, the INGD update of \mathbf{K} without Riemannian momentum (i.e., $\alpha_1 = 0$) is

$$\mathbf{K}^{\text{new}} \leftarrow \mathbf{K} \left[\mathbf{I}_{d_i} - \frac{\beta_1}{2d_o} (\text{Tr}(\mathbf{H}_C) \mathbf{H}_K + \lambda \text{Tr}(\mathbf{C}^\top \mathbf{C}) \mathbf{K}^\top \mathbf{K} - d_o \mathbf{I}_{d_i}) \right]. \quad (9)$$

Notice that $\text{Tr}(\mathbf{I}_{d_o}) = d_o$, $\mathbf{H}_C \in \mathbb{R}^{d_o \times d_o}$, $\mathbf{C} \in \mathbb{R}^{d_o \times d_o}$, and $\mathbf{K} \in \mathbb{R}^{d_i \times d_i}$. Thus, we can obtain IKFAC from INGD (shown in Fig. 3) by simply replacing $\text{Tr}(\mathbf{H}_C)$ and $\text{Tr}(\mathbf{C}^\top \mathbf{C})$ with $\text{Tr}(\mathbf{I}_{d_o})$:

$$\mathbf{K}^{\text{new}} \leftarrow \mathbf{K} \left[\mathbf{I}_{d_i} - \frac{\beta_1}{2d_o} (\text{Tr}(\mathbf{I}_{d_o}) \mathbf{H}_K + \lambda \text{Tr}(\mathbf{I}_{d_o}) \mathbf{K}^\top \mathbf{K} - d_o \mathbf{I}_{d_i}) \right]. \quad (10)$$

This also sheds light on the difference between INGD and KFAC. In IKFAC (see Appendix D for the details), \mathbf{H}_K and $\lambda \mathbf{K}^\top \mathbf{K}$ are used for incorporating curvature \mathbf{U} and damping $\lambda \mathbf{I}$ in the KFAC update, respectively. In contrast, the curvature and damping is *adaptively* incorporated in INGD using $(\text{Tr}(\mathbf{H}_C)/d_o) \mathbf{H}_K$ and $(\lambda \text{Tr}(\mathbf{C}^\top \mathbf{C})/d_o) \mathbf{K}^\top \mathbf{K}$. The updates of \mathbf{K} and \mathbf{C} are *correlated* in INGD due to the trace terms. In contrast, \mathbf{K} and \mathbf{C} are updated independently in IKFAC—just like \mathbf{S}_K and \mathbf{S}_C are updated independently in KFAC. These trace terms are needed to satisfy the orthonormalization condition of the Fisher matrix (Lin et al., 2023). Those trace terms make INGD and SINGD scale invariant to the Kronecker approximation (see Appx. F) as the approximation is not unique. In contrast, KFAC and IKFAC are not scale invariant to the Kronecker approximation. The trace terms together with Riemannian momentum (i.e., $\alpha_1 > 0$) are missing in KFAC and IKFAC. Our experiments show that these terms can contribute to stability of INGD over KFAC and IKFAC.

3.2 SPARSE KRONECKER FACTORS FOR REDUCING MEMORY

We extend the INGD method to reduce memory consumption and lower the iteration cost for training large NNs such as transformer-based models. We propose using sparse Kronecker factors \mathbf{K} and \mathbf{C} in INGD. In contrast, existing structured KFAC methods (Zhang et al., 2019; Grosse et al., 2023) consider (block-)diagonal structures of factors \mathbf{S}_K and \mathbf{S}_C . These simple structures may compromise downstream performance. Unfortunately, explicitly imposing more flexible structures on factors \mathbf{S}_K and \mathbf{S}_C can be either computationally challenging, memory inefficient, or numerically unstable. Other related works are Lie group preconditioners (Li, 2018; 2022) derived from directly approximating the Hessian. However, these methods can be computationally expensive and numerically unstable since generating random weight matrices and solving linear systems (i.e., matrix inversions) required by their methods are not stable in low precision settings.

Sparse factors \mathbf{K} and \mathbf{C} can be useful as they enable us to use more flexible structures (illustrated in Fig. 5) and achieve better downstream performance than (block-)diagonal structures. For example, a sparse factor \mathbf{K} (see the leftmost plot of Fig. 8) can enforce a diagonal-plus-rank-one (dense) structure (Lin et al., 2021) in \mathbf{S}_K as we use $\mathbf{K} \mathbf{K}^\top$ in the inverse-free KFAC update to approximate $(\mathbf{S}_K + \lambda \mathbf{I})^{-1}$ in the KFAC update in Sec. 3.1. Similarly, another sparse factor \mathbf{K} (see the rightmost plot of Fig. 8) can introduce a diagonal-plus-rank-one (dense) structure in the inverse of \mathbf{S}_K . In contrast, explicitly imposing such a structure on \mathbf{S}_K or its inverse could be memory inefficient.

As a general design principle, we consider special structures preserved under (1) elementwise matrix operations (e.g., matrix subtraction and scalar multiplication) and (2) matrix multiplication. These operations are needed for our updates. We exploit Lie-algebraic properties in the matrix logarithm space to construct sparse structures² of Kronecker factors \mathbf{K} and \mathbf{C} . We construct a structure³ by using a subspace of the logarithm space. Concretely, we construct a new local reparameterization map for \mathbf{K} at iteration t such as $\mathbf{K} := \psi(\mathbf{K}_t, \mathbf{m}_K) := \mathbf{K}_t \text{Expm}(1/(2\sqrt{d_i}) \hat{\Pi}_K(\mathbf{m}_K))$, where map $\hat{\Pi}_K(\mathbf{m}_K)$ projects dense input \mathbf{m}_K onto a subspace. We specify a subspace so that its sparse pattern is preserved under matrix multiplication and the elementwise matrix operations.

It can be non-trivial to design such a sparse factor while maintaining downstream performance. For example, many well-known sparse factors such as tri-diagonal matrices do not satisfy our requirements as they are not closed under matrix multiplication. Moreover, it can be difficult to construct the projection map so that the orthonormalization condition (Lin et al., 2023) of the FIM is

²These (Lie-group) structures are preserved even under matrix inversion and matrix exponential.

³Each matrix (Lie-group) structure is induced by a subspace of Lie-algebra of the general linear group.

Subspace of the logarithm space (Lie algebra)	Lie (sub-group) structure in \mathbf{K}	Subspace projection map $\hat{\Pi}(\mathbf{m})$
$\begin{bmatrix} a_{1,1} & 0 & \cdots & 0 \\ a_{2,1} & a_{2,2} & & 0 \\ \vdots & \vdots & \ddots & \vdots \\ a_{d_i,1} & a_{d_i,2} & \cdots & a_{d_i,d_i} \end{bmatrix}$	Lower-triangular (Tril.)	$\begin{bmatrix} m_{1,1} & 0 & \cdots & 0 \\ 2m_{2,1} & m_{2,2} & & 0 \\ \vdots & \vdots & \ddots & \vdots \\ 2m_{d_i,1} & 2m_{d_i,2} & \cdots & m_{d_i,d_i} \end{bmatrix}$
$\begin{bmatrix} \mathbf{A}_{11} & 0 & \cdots & 0 \\ 0 & \mathbf{A}_{22} & \cdots & 0 \\ \vdots & \vdots & \ddots & \vdots \\ 0 & 0 & \cdots & \mathbf{A}_{qq} \end{bmatrix}$	(Block) Diagonal (k is the block size)	$\begin{bmatrix} \mathbf{M}_{11} & 0 & \cdots & 0 \\ 0 & \mathbf{M}_{22} & \cdots & 0 \\ \vdots & \vdots & \ddots & \vdots \\ 0 & 0 & \cdots & \mathbf{M}_{qq} \end{bmatrix}$
$\begin{bmatrix} \mathbf{A}_{11} & \mathbf{A}_{12} & \mathbf{A}_{13} \\ 0 & \mathbf{A}_{22} & 0 \\ 0 & \mathbf{A}_{32} & \mathbf{A}_{33} \end{bmatrix}$, \mathbf{A}_{22} is diag., $\mathbf{A}_{11} \in \mathcal{R}^{d_2 \times d_2}$, $\mathbf{A}_{33} \in \mathcal{R}^{d_3 \times d_3}$	Hierarchical ($k := d_2 + d_3$)	$\begin{bmatrix} \mathbf{M}_{11} & 2\mathbf{M}_{12} & 2\mathbf{M}_{13} \\ 0 & \text{Diag}(\mathbf{M}_{22}) & 0 \\ 0 & 2\mathbf{M}_{32} & \mathbf{M}_{33} \end{bmatrix}$
$\begin{bmatrix} \mathbf{A}_{11} & \mathbf{A}_{12} \\ 0 & \mathbf{D}_{22} \end{bmatrix}$, \mathbf{D}_{22} is diag., $\mathbf{A}_{11} \in \mathcal{R}^{k \times k}$	Rank- k lower-triangular	$\begin{bmatrix} \mathbf{M}_{11} & 2\mathbf{M}_{12} \\ 0 & \text{Diag}(\mathbf{M}_{22}) \end{bmatrix}$
$\begin{bmatrix} a_0 & a_1 & a_2 & \cdots & a_{(d_i-1)} \\ 0 & a_0 & a_1 & \ddots & \vdots \\ 0 & 0 & \ddots & \ddots & a_2 \\ \vdots & \ddots & \ddots & \ddots & a_1 \\ 0 & \cdots & \ddots & 0 & a_0 \end{bmatrix}$	Upper-triangular Toeplitz (Triu-Toepl.)	$\begin{bmatrix} b_0 & 2b_1 & 2b_2 & \cdots & 2b_{(d_i-1)} \\ 0 & b_0 & 2b_1 & \ddots & \vdots \\ 0 & 0 & \ddots & \ddots & 2b_2 \\ \vdots & \ddots & \ddots & \ddots & 2b_1 \\ 0 & \cdots & \cdots & 0 & b_0 \end{bmatrix}$ $b_j := \frac{1}{d_i-j} \sum_{k=1}^{d_i-j} m_{k,k+j}$

Table 1: Subspaces of the logarithm space and their projection maps $\hat{\Pi}(\mathbf{m})$, where \mathbf{m} is a symmetry matrix. The hierarchical structure is constructed by replacing the diagonal matrix \mathbf{D}_{22} in the rank- k lower-triangular structure with another rank- k triangular matrix $\begin{bmatrix} \mathbf{A}_{22} & 0 \\ \mathbf{A}_{23} & \mathbf{A}_{33} \end{bmatrix}$ for a better approximation.

satisfied. We would have to compute the inverse of the FIM if the orthonormalization condition is not satisfied.

One particular subspace structure satisfying these requirements is the class of upper/lower triangular matrices⁴. In the triangular case, the subspace projection $\hat{\Pi}_K$ is a weighted extraction map since projecting the logarithm space onto a subspace is like projecting a dense square matrix onto a triangular matrix space. The logarithm space arising from the dense case is an ordinary (Euclidean) matrix space because the Fisher block with respect to \mathbf{K} at $\mathbf{m}_K = \mathbf{0}$ is locally orthonormalized. The subspace projection is a weighted map since it has to satisfy the orthonormalization condition in the subspace. Technically, we consider the factor $\mathbf{A} := \mathbf{K}_t \text{Expm}(\hat{\Pi}_K(\mathbf{m}_K)/(2\sqrt{d_i})) \otimes \mathbf{C}_t$ to update \mathbf{K} at iteration t , where \mathbf{C}_t and \mathbf{K}_t are treated as constants. Given a subspace $\Omega_K \subset \mathbb{R}^{d_i \times d_i}$ in the matrix logarithm space, the subspace projection map $\hat{\Pi}_K : \text{Sym}^{d_i \times d_i} \mapsto \Omega_K$ is specified by satisfying the local orthonormalization condition (Lin et al., 2023) of the Fisher block with respect to \mathbf{m}_K : $F(\mathbf{m}_K)|_{\mathbf{m}_K=\mathbf{0}} := -\mathbb{E}_{w \sim q} [\nabla_{\mathbf{m}_K}^2 \log q(\mathbf{w}|\boldsymbol{\mu}, \mathbf{S})]|_{\mathbf{m}_K=\mathbf{0}} = \mathbf{I}$, where $q(\mathbf{w}|\boldsymbol{\mu}, \mathbf{S})$ is the variational Gaussian with mean $\boldsymbol{\mu}$ and precision $\mathbf{S} := \mathbf{A}^{-T} \mathbf{A}^{-1}$ and $\text{Sym}^{d_i \times d_i}$ denotes the set of symmetric square real matrices. Similarly, we can obtain the subspace projection for \mathbf{C} (Lin et al., 2023) by using $\mathbf{A} := \mathbf{K}_t \otimes \mathbf{C}_t \text{Expm}(\hat{\Pi}_C(\mathbf{m}_C)/(2\sqrt{d_o}))$ to satisfy the orthonormalization condition with respect to \mathbf{m}_C .

We consider several sparse structures and block extensions of the triangular matrix class as illustrated in Fig. 5. For example, the subspace projection map for a diagonal structure simply extracts diagonal entries of its input. As a non-trivial example, the subspace projection map for a lower-triangular structure extracts lower-triangular entries of its input and multiplies the entries below the main diagonal by 2. Table 1 summarizes structures and their projection maps considered in this work. Our framework allows us to include flexible structures such as the hierarchical structure. Many existing second-order methods focus on low-rank structures while our method supports not only low-rank structures (see Fig. 8) but also other sparse structures such as Toeplitz structures. For an efficient implementation, we only compute and store non-zero entries of $\hat{\Pi}_K(\mathbf{m}_K)$ and \mathbf{K} without explicitly forming dense matrices \mathbf{m}_K and \mathbf{K} .

By using such a subspace and its projection map, we obtain a structured INGD update scheme (see Fig. 4). We can also obtain a structured version of IKFAC. Our approach allows us to use more expressive structures than the block-diagonal structure as illustrated in Fig. 5 and 8. These structures lower not only memory consumption (shown in Table 3) but also the iteration cost (shown in Table 2).

⁴This class forms a matrix associative (sub)algebra.

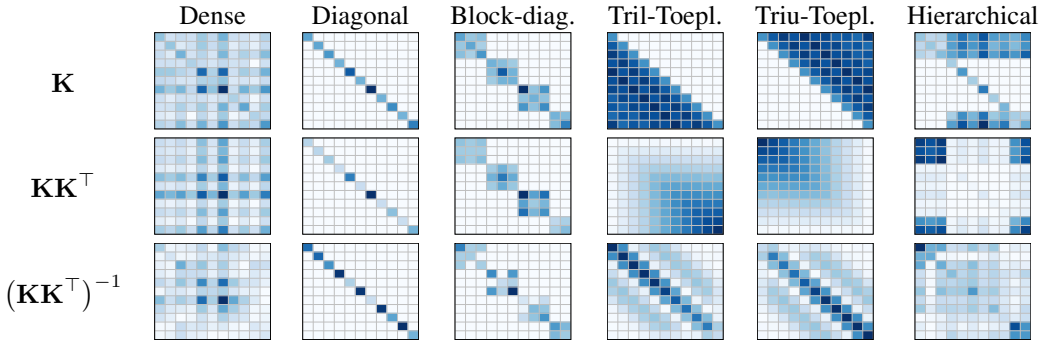


Figure 5: Illustration of structured matrices (Kronecker factors) supported by SINGD, their self-outer product (approximate inverse Hessian factor), and its inverse (approximate Hessian factor).

4 EXPERIMENTS

To demonstrate the robustness and memory efficiency of our method, we consider image classification tasks with transformer-based models such as “Compact-ViT” (Hassani et al., 2021), “Swin-ViT” (Liu et al., 2021), “GC-ViT” (Hatamizadeh et al., 2023), and “HDVT” (Lu et al., 2022). We also consider convolution-based models such as “VGG” (Simonyan & Zisserman, 2014), “ConvMixer” (Trockman & Kolter, 2023), and “Rep-ViT” (Wang et al., 2023). We train these models on datasets “CIFAR-100” and “ImageWoof-10”. Note that “Rep-ViT” is a CNN model inspired by transformers while “Compact-ViT” is a data-efficient transformer using convolutional tokenization. We also consider a graph convolution model (Kipf & Welling, 2016) denoted by “GNN” for node classification on dataset “Cora”.

To be memory efficient, we consider SINGD with sparse structures such as “diagonal”, “block-diagonal”, and “hierarchical”. We also consider IKFAC, INGD, and AdamW as our baselines. Recall that our method becomes INGD if we use a dense structure. We use a random search to find the best hyper-parameters of each of the methods. We use mixed-precision training with BFP16 and cosine step-size schedules for our experiments. We use KFAC-reduce (Eschenhagen et al., 2023) and numerical tricks (Dangel, 2023) to further reduce memory consumption and the iteration cost for convolutions. All methods except KFAC directly support training with BFP16. For KFAC, we have to first transform a matrix into FP32 and then transform the inverse of the matrix into BFP16 when using matrix inversion. We find out that KFAC performs unstably in BFP16. For “VGG” and “ConvMixer”, we also consider SGD as a strong baseline. We fix the momentum weight to be 0.9 and tune other hyper-parameters of each optimizer using random search. For “VGG” and “ConvMixer”, we decrease learning rate β_2 every 40 epochs. For “GNN”, we use a constant learning rate. For the rest of the models including all the transformer-based models, we use a cosine learning rate schedule. We consider KFAC as a strong baseline for the GNN model as suggested by Izadi et al. (2020). We train the GNN model with FP32 so that KFAC performs stably in this case. The list of hyper-parameters used in the random search can be found in Table 4 in Appendix C. We use the test error to measure the performance of each method.

From Fig. 6 and 7, we can observe that SINGD including IKFAC and INGD as special cases, outperforms AdamW in many cases. SINGD works well for mixed-precision training. We do not show KFAC in the plots as it performs unstably due to numerical issues. We also observe that the hierarchical structure often performs as well as the dense structure (INGD) on all the models. In several cases, the hierarchical structure outperforms the block-diagonal and diagonal structures. However, on the models as shown in Fig. 7, even the diagonal structure can perform as well as the dense structure. Thus, we can reduce the memory consumption of INGD and make SINGD as competitive as AdamW for training large NNs.

5 CONCLUSIONS

We propose an inverse-free, memory-efficient natural gradient descent method—SINGD—which addresses the numerical instability and memory inefficiency of contemporary second-order methods like KFAC (Martens & Grosse, 2015). The algorithm is an extension of the inverse-free natural gradient (INGD) method from Lin et al. (2023), whose update relies only on matrix multiplications.

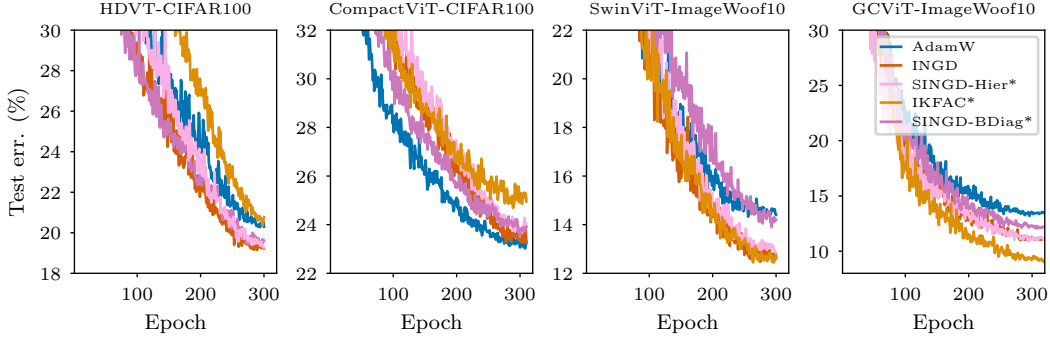


Figure 6: Test error curves for mixed-precision training in the transformer-based models with BFP16 on datasets “CIFAR-100” and “ImageWoof-10”. Note that “Compact-ViT” and “HDVT” are data-efficient transformers. Our method (SINGD) performs as well as INGD while being memory efficient. SINGD including IKFAC and INGD as special cases, outperforms AdamW in most of the cases. We do not show KFAC in the plots since it performs unstably in BFP16. The hierarchical structure often performs as well as the dense structure and outperforms the block-diagonal structure.

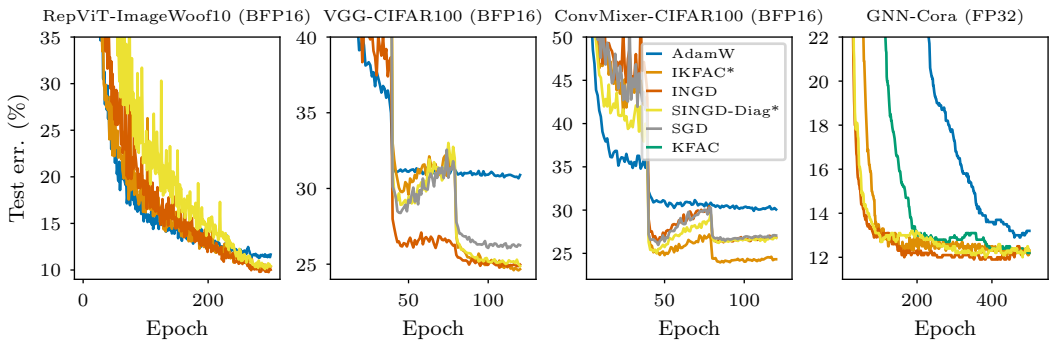


Figure 7: Test error curves for mixed-precision training in CNN and GNN models on datasets “ImageWoof-10”, “CIFAR-100” and “Cora”. Note that “Rep-ViT” is a CNN model inspired by transformers. Our method (SINGD) performs as well as INGD while being memory efficient. SINGD including IKFAC and INGD as special cases, outperforms AdamW on all the models. The diagonal structure can perform as well as the dense structure on these models. KFAC only appears in the rightmost plot since it performs unstably in the other plots due to numerical issues in half-precision settings.

We theoretically establish the algorithm’s relation to KFAC by showing that a modification of INGD effectively performs KFAC-like updates. Then, we improve its memory efficiency through sparse Kronecker factors. Our experiments show that our method supports low-precision training and often outperforms AdamW for modern architecture such as transformer-based models. Our work expands the scope of second-order methods to training transformer-based NNs and training in low precision, making them more widely applicable than before.

Future work: We plan to exploit SINGD’s low memory footprint and numerical stability to train large language models. Our experiments also suggest that SINGD might be able to train a wide range of architectures, which should be investigated further, e.g. by evaluating it on the AlgoPerf training algorithms benchmark (Dahl et al., 2023).

ACKNOWLEDGMENTS

Resources used in preparing this research were provided, in part, by the Province of Ontario, the Government of Canada through CIFAR, and companies sponsoring the Vector Institute.

REFERENCES

Shun-Ichi Amari. Natural gradient works efficiently in learning. *Neural computation*, 10(2):251–276, 1998.

Juhan Bae, Nathan Ng, Alston Lo, Marzyeh Ghassemi, and Roger B Grosse. If influence functions are the answer, then what is the question? In *NeurIPS*, 2022.

Aleksandar Botev, Hippolyt Ritter, and David Barber. Practical Gauss-Newton optimisation for deep learning. In *ICML*, 2017.

James Bradbury, Roy Frostig, Peter Hawkins, Matthew James Johnson, Chris Leary, Dougal Maclaurin, George Necula, Adam Paszke, Jake VanderPlas, Skye Wanderman-Milne, and Qiao Zhang. JAX: composable transformations of Python+NumPy programs, 2018. URL <http://github.com/google/jax>.

Tom Brown, Benjamin Mann, Nick Ryder, Melanie Subbiah, Jared D Kaplan, Prafulla Dhariwal, Arvind Neelakantan, Pranav Shyam, Girish Sastry, Amanda Askell, et al. Language models are few-shot learners. In *NeurIPS*, 2020.

George E. Dahl, Frank Schneider, Zachary Nado, Naman Agarwal, Chandramouli Shama Sastry, Philipp Hennig, Sourabh Medapati, Runa Eschenhagen, Priya Kasimbeg, Daniel Suo, Juhan Bae, Justin Gilmer, Abel L. Peirson, Bilal Khan, Rohan Anil, Mike Rabbat, Shankar Krishnan, Daniel Snider, Ehsan Amid, Kongtao Chen, Chris J. Maddison, Rakshith Vasudev, Michal Badura, Ankush Garg, and Peter Mattson. Benchmarking neural network training algorithms. arXiv 2306.07179, 2023.

Felix Dangel. Convolutions through the lens of tensor networks. arXiv 2307.02275, 2023.

Erik Daxberger, Agustinus Kristiadi, Alexander Immer, Runa Eschenhagen, Matthias Bauer, and Philipp Hennig. Laplace redux—effortless Bayesian deep learning. In *NeurIPS*, 2021.

Mostafa Dehghani, Josip Djolonga, Basil Mustafa, Piotr Padlewski, Jonathan Heek, Justin Gilmer, Andreas Peter Steiner, Mathilde Caron, Robert Geirhos, Ibrahim Alabdulmohsin, et al. Scaling vision transformers to 22 billion parameters. In *ICML*, 2023.

Runa Eschenhagen, Alexander Immer, Richard E. Turner, Frank Schneider, and Philipp Hennig. Kronecker-Factored Approximate Curvature for modern neural network architectures. In *NeurIPS*, 2023.

Thomas George, César Laurent, Xavier Bouthillier, Nicolas Ballas, and Pascal Vincent. Fast approximate natural gradient descent in a kronecker factored eigenbasis. In *NeurIPS*, 2018.

Alex Graves. Practical variational inference for neural networks. In *NeurIPS*, 2011.

Roger Grosse and James Martens. A kronecker-factored approximate fisher matrix for convolution layers. In *ICML*, 2016.

Roger Grosse, Juhan Bae, Cem Anil, Nelson Elhage, Alex Tamkin, Amirhossein Tajdini, Benoit Steiner, Dustin Li, Esin Durmus, Ethan Perez, et al. Studying large language model generalization with influence functions. *arXiv preprint arXiv:2308.03296*, 2023.

Ali Hassani, Steven Walton, Nikhil Shah, Abulikemu Abuduweili, Jiachen Li, and Humphrey Shi. Escaping the big data paradigm with compact transformers. *arXiv preprint arXiv:2104.05704*, 2021.

Ali Hatamizadeh, Hongxu Yin, Greg Heinrich, Jan Kautz, and Pavlo Molchanov. Global context vision transformers. In *International Conference on Machine Learning*, pp. 12633–12646. PMLR, 2023.

Tom Heskes. On “natural” learning and pruning in multilayered perceptrons. *Neural Computation*, 12(4), 2000.

Alexander Immer, Matthias Bauer, Vincent Fortuin, Gunnar Rätsch, and Khan Mohammad Emtiyaz. Scalable marginal likelihood estimation for model selection in deep learning. In *ICML*, 2021.

Mohammad Rasool Izadi, Yihao Fang, Robert Stevenson, and Lizhen Lin. Optimization of graph neural networks with natural gradient descent. In *2020 IEEE international conference on big data (big data)*, pp. 171–179. IEEE, 2020.

Mohammad Khan and Wu Lin. Conjugate-computation variational inference: Converting variational inference in non-conjugate models to inferences in conjugate models. In *Artificial Intelligence and Statistics*, pp. 878–887, 2017.

Mohammad Emtiyaz Khan and Håvard Rue. The bayesian learning rule. *arXiv preprint arXiv:2107.04562*, 2021.

Mohammad Emtiyaz Khan, Didrik Nielsen, Voot Tangkaratt, Wu Lin, Yarin Gal, and Akash Srivastava. Fast and scalable Bayesian deep learning by weight-perturbation in Adam. In *ICML*, 2018.

Diederik P Kingma and Jimmy Ba. Adam: A method for stochastic optimization. In *International Conference on Learning Representations*, 2015.

Thomas N Kipf and Max Welling. Semi-supervised classification with graph convolutional networks. *arXiv preprint arXiv:1609.02907*, 2016.

Frederik Kunstner, Lukas Balles, and Philipp Hennig. Limitations of the empirical Fisher approximation for natural gradient descent. In *NeurIPS*, 2019.

Xi-Lin Li. Preconditioner on matrix lie group for sgd. In *International Conference on Learning Representations*, 2018.

Xilin Li. Black box lie group preconditioners for sgd. *arXiv preprint arXiv:2211.04422*, 2022.

Wu Lin, Mark Schmidt, and Mohammad Emtiyaz Khan. Handling the positive-definite constraint in the bayesian learning rule. In *ICML*, 2020.

Wu Lin, Frank Nielsen, Khan Mohammad Emtiyaz, and Mark Schmidt. Tractable structured natural-gradient descent using local parameterizations. In *ICML*, 2021.

Wu Lin, Valentin Duruisseaux, Melvin Leok, Frank Nielsen, Mohammad Emtiyaz Khan, and Mark Schmidt. Simplifying momentum-based positive-definite submanifold optimization with applications to deep learning. 2023.

Ze Liu, Yutong Lin, Yue Cao, Han Hu, Yixuan Wei, Zheng Zhang, Stephen Lin, and Baining Guo. Swin transformer: Hierarchical vision transformer using shifted windows. In *Proceedings of the IEEE/CVF international conference on computer vision*, pp. 10012–10022, 2021.

Ilya Loshchilov and Frank Hutter. Decoupled weight decay regularization. In *ICLR*, 2019.

Zhiying Lu, Hongtao Xie, Chuanbin Liu, and Yongdong Zhang. Bridging the gap between vision transformers and convolutional neural networks on small datasets. *Advances in Neural Information Processing Systems*, 35:14663–14677, 2022.

James Martens. New insights and perspectives on the natural gradient method. *JMLR*, 21(146), 2014.

James Martens and Roger Grosse. Optimizing neural networks with Kronecker-factored approximate curvature. In *ICML*, 2015.

James Martens, Jimmy Ba, and Matt Johnson. Kronecker-factored curvature approximations for recurrent neural networks. In *ICLR*, 2018.

Paulius Micikevicius, Sharan Narang, Jonah Alben, Gregory Diamos, Erich Elsen, David Garcia, Boris Ginsburg, Michael Houston, Oleksii Kuchaiev, Ganesh Venkatesh, and Hao Wu. Mixed precision training. In *International Conference on Learning Representations (ICLR)*, 2018.

Kazuki Osawa, Siddharth Swaroop, Mohammad Emtiyaz E Khan, Anirudh Jain, Runa Eschenhagen, Richard E Turner, and Rio Yokota. Practical deep learning with Bayesian principles. In *NeurIPS*, 2019.

Kazuki Osawa, Shigang Li, and Torsten Hoefler. PipeFisher: Efficient training of large language models using pipelining and Fisher information matrices. In *MLSys*, 2023.

Michael R Osborne. Fisher’s method of scoring. *International Statistical Review/Revue Internationale de Statistique*, pp. 99–117, 1992.

Adam Paszke, Sam Gross, Francisco Massa, Adam Lerer, James Bradbury, Gregory Chanan, Trevor Killeen, Zeming Lin, Natalia Gimelshein, Luca Antiga, et al. PyTorch: An imperative style, high-performance deep learning library. In *NeurIPS*, 2019.

Alec Radford, Jeffrey Wu, Rewon Child, David Luan, Dario Amodei, Ilya Sutskever, et al. Language models are unsupervised multitask learners. *OpenAI blog*, 1(8):9, 2019.

Herbert Robbins and Sutton Monro. A Stochastic Approximation Method. *The Annals of Mathematical Statistics*, 1951.

Nicol N Schraudolph. Fast curvature matrix-vector products for second-order gradient descent. *Neural computation*, 14(7), 2002.

Karen Simonyan and Andrew Zisserman. Very deep convolutional networks for large-scale image recognition. *arXiv preprint arXiv:1409.1556*, 2014.

Gordon K Smyth. Partitioned algorithms for maximum likelihood and other non-linear estimation. *Statistics and Computing*, 6:201–216, 1996.

Gordon K Smyth. Optimization and nonlinear equations. *Statistics reference online*, 1:1–9, 2015.

Linda SL Tan. Analytic natural gradient updates for cholesky factor in gaussian variational approximation. *arXiv preprint arXiv:2109.00375*, 2022.

Neil C Thompson, Kristjan Greenewald, Keeheon Lee, and Gabriel F Manso. The computational limits of deep learning. 2020.

Hugo Touvron, Thibaut Lavril, Gautier Izacard, Xavier Martinet, Marie-Anne Lachaux, Timothée Lacroix, Baptiste Rozière, Naman Goyal, Eric Hambro, Faisal Azhar, et al. LLaMA: Open and efficient foundation language models. *arXiv preprint arXiv:2302.13971*, 2023.

Asher Trockman and J Zico Kolter. Patches are all you need? *Transactions on Machine Learning Research*, 2023.

Ashish Vaswani, Noam Shazeer, Niki Parmar, Jakob Uszkoreit, Llion Jones, Aidan N Gomez, Łukasz Kaiser, and Illia Polosukhin. Attention is all you need. In *NIPS*, 2017.

Ao Wang, Hui Chen, Zijia Lin, Hengjun Pu, and Guiguang Ding. Repvit: Revisiting mobile cnn from vit perspective. *arXiv preprint arXiv:2307.09283*, 2023.

Chaoqi Wang, Roger Grosse, Sanja Fidler, and Guodong Zhang. Eigendamage: Structured pruning in the kronecker-factored eigenbasis. In *ICML*, 2019.

Yong Wang. Fisher scoring: An interpolation family and its Monte Carlo implementations. *Comput. Stat. Data Anal.*, 54(7), 2010.

Guodong Zhang, Shengyang Sun, David Duvenaud, and Roger Grosse. Noisy natural gradient as variational inference. In *ICML*, 2018.

Guodong Zhang, Lala Li, Zachary Nado, James Martens, Sushant Sachdeva, George E. Dahl, Christopher J. Shallue, and Roger B. Grosse. Which algorithmic choices matter at which batch sizes? Insights from a noisy quadratic model. In *NeurIPS*, 2019.

Appendices

A SPACE AND TIME COMPLEXITY

	Method	$\Delta\mu$ (descent direction)	Update \mathbf{S}_K or \mathbf{K}	Update \mathbf{S}_C or \mathbf{C}	$\nabla_\mu \ell$ (BackProp)
Iteration Cost	KFAC	$O(d_i^2 d_o + d_o^2 d_i)$	$O(\frac{1}{T}(md_i^2 + d_o^3))$	$O(\frac{1}{T}(md_o^2 + d_o^3))$	$O(md_i d_o)$
	INGD/SINGD (Dense)	$O(d_i^2 d_o + d_o^2 d_i)$	$O(\frac{1}{T}(md_i^2 + d_o^3))$	$O(\frac{1}{T}(md_o^2 + d_o^3))$	$O(md_i d_o)$
	SINGD (Block-Diag. with block size k)	$O(kd_i d_o)$	$O(\frac{1}{T}(kmd_i))$	$O(\frac{1}{T}(kmd_o))$	$O(md_i d_o)$
	SINGD (Toeplitz)	$O(d_i d_o \log(d_o d_i))$	$O(\frac{1}{T}(md_i \log d_i))$	$O(\frac{1}{T}(md_o \log d_o))$	$O(md_i d_o)$
	SINGD (Rank-1 Triangular)	$O(d_i d_o)$	$O(\frac{1}{T}(md_i))$	$O(\frac{1}{T}(md_o))$	$O(md_i d_o)$
	SINGD (Hierarchical with parameter k)	$O(kd_i d_o)$	$O(\frac{1}{T}(kmd_i))$	$O(\frac{1}{T}(kmd_o))$	$O(md_i d_o)$
	AdamW	$O(d_i d_o)$	NA	NA	$O(md_i d_o)$

Table 2: Iteration cost for a non-weight-sharing layer, where m is the size of a mini-batch and $\mu \in \mathbb{R}^{d_i \times d_o}$ is a learnable weight matrix.

	Method	$\nabla_\mu \ell \odot \nabla_\mu \ell$	\mathbf{S}_K or \mathbf{K}	\mathbf{S}_C or \mathbf{C}
Memory Usage	KFAC	NA	$O(d_i^2)$	$O(d_o^2)$
	INGD/SINGD (Dense)	NA	$O(d_i^3)$	$O(d_o^3)$
	SINGD (Block-Diag. with block size k)	NA	$O(kd_i)$	$O(kd_o)$
	SINGD (Toeplitz)	NA	$O(d_i)$	$O(d_o)$
	SINGD (Rank-1 Triangular)	NA	$O(d_i)$	$O(d_o)$
	SINGD (Hierarchical with parameter k)	NA	$O(kd_i)$	$O(kd_o)$
	AdamW	$O(d_i d_o)$	NA	NA

Table 3: Additional Storage

B MORE SPARSE STRUCTURES

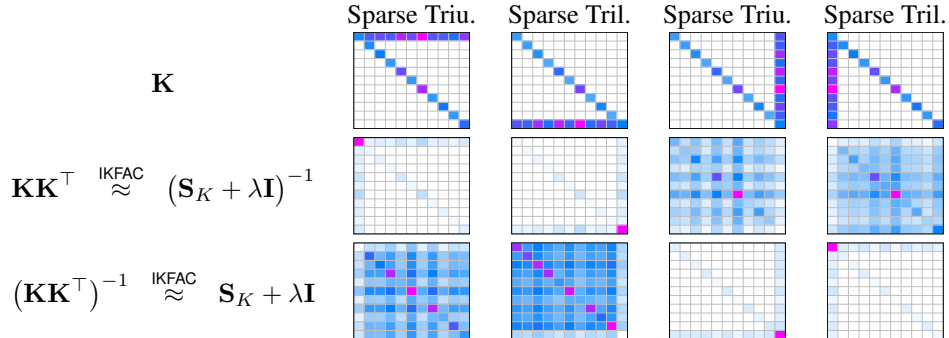


Figure 8: Our approach can impose a low-rank (dense) structure on \mathbf{KK}^\top or its inverse using rank-one triangular matrices \mathbf{K} . It can be difficult to directly impose a low-rank structure on $(\mathbf{S}_K + \lambda \mathbf{I})^{-1}$.

C DETAILS OF THE EXPERIMENTS

INGD	AdamW Optimizer
<p>1: Each T iter., update $\mathbf{m}_K, \mathbf{m}_C, \mathbf{K}, \mathbf{C}$ Obtain $\mu_{AA} \otimes \mu_{GG}$ to approximate $\nabla_\mu^2 \ell(\mu)$ $\mathbf{m}_K \leftarrow \alpha_1 \mathbf{m}_K + \frac{\beta_1}{2d} (\text{Tr}(\mathbf{H}_C) \mathbf{H}_K + c^2 \mathbf{K}^T \mathbf{K} - d \mathbf{I}_p)$ $\mathbf{m}_C \leftarrow \alpha_1 \mathbf{m}_C + \frac{\beta_1}{2p} (\text{Tr}(\mathbf{H}_K) \mathbf{H}_C + \kappa^2 \mathbf{C}^T \mathbf{C} - p \mathbf{I}_d)$ $\mathbf{K} \leftarrow \mathbf{K} \text{Exp}(-\mathbf{m}_K) \approx \mathbf{K}(\mathbf{I}_p - \mathbf{m}_K)$ $\mathbf{C} \leftarrow \mathbf{C} \text{Exp}(-\mathbf{m}_C) \approx \mathbf{C}(\mathbf{I}_d - \mathbf{m}_C)$</p> <p>2: $\mathbf{M}_\mu \leftarrow \alpha_2 \mathbf{M}_\mu + \mathbf{C} \mathbf{C}^T \text{vec}^{-1}(\nabla_\mu \ell(\mu)) \mathbf{K} \mathbf{K}^T + \gamma \text{vec}^{-1}(\mu)$</p> <p>3: $\mu \leftarrow \mu - \beta_2 \text{vec}(\mathbf{M}_\mu)$</p>	<p>1: At iter. t, update \mathbf{m}_s, \mathbf{s} Use $(\nabla_\mu \ell(\mu))^2$ to approximate $\text{diag}(\nabla_\mu^2 \ell(\mu))$ $\mathbf{m}_s \leftarrow (1 - \beta_1) \mathbf{m}_s + \beta_1 (\nabla_\mu \ell(\mu))^2$ $\mathbf{s}^2 \leftarrow \mathbf{m}_s / (1 - (1 - \beta_1)^t)$ $\mathbf{s} \leftarrow \sqrt{\mathbf{s}^2} + \lambda$</p> <p>2: $\mathbf{m}_\mu \leftarrow \alpha_2 \mathbf{m}_\mu + (1 - \alpha_2) \nabla_\mu \ell(\mu)$ $\mathbf{M}_\mu \leftarrow \mathbf{s}^{-1} \mathbf{m}_\mu / (1 - \alpha_2^t)$</p> <p>3: $\mu \leftarrow \mu - \beta_2 \mathbf{M}_\mu + \gamma \mu$</p>

Figure 9: Baseline methods in the same notation for a hyperparameter search.

Hyperparameter	Meaning	KFAC/IKFAC/SINGD in Fig. 4 and 9	AdamW in Fig. 9
β_2	Standard stepsize	Tuned	Tuned
α_2	Standard momentum weight	0.9	0.9
γ	(L2) weight decay	Tuned	Tuned
λ	Damping	Tuned	Tuned
β_1	Stepsize for preconditioner	Tuned	Tuned
α_1	Riemannian Momentum	(SINGD only) Tuned	NA

Table 4: Hyperparameters used for a random search.

D CONNECTION BETWEEN IKFAC AND KFAC

To relate to the KFAC method, we now show that $\mathbf{K}^{\text{new}}(\mathbf{K}^{\text{new}})^\top$ is an approximation of $(\mathbf{S}_K^{\text{new}} + \lambda\mathbf{I})^{-1}$ at a new step of our scheme. For simplicity, we first assume $\mathbf{K}\mathbf{K}^\top$ exactly equals to $(\mathbf{S}_K^{\text{cur}} + \lambda\mathbf{I})^{-1}$ at the current step. Later, we will relax this assumption and prove that $\mathbf{K}\mathbf{K}^\top$ is an approximation of $(\mathbf{S}_K + \lambda\mathbf{I})^{-1}$ at every step as stated in Theorem 1. For notation simplicity, we denote $\bar{\mathbf{S}}_K := \mathbf{S}_K + \lambda\mathbf{I}$. The update of \mathbf{S}_K with damping $\lambda\mathbf{I}$ can be reexpressed as an update of $\bar{\mathbf{S}}_K$:

$$(\mathbf{S}_K^{\text{new}} + \lambda\mathbf{I}) = \bar{\mathbf{S}}_K^{\text{new}} \leftarrow (1 - \beta_1)\bar{\mathbf{S}}_K^{\text{cur}} + \beta_1(\mathbf{U} + \lambda\mathbf{I}).$$

Since $\hat{\mathbf{S}}_K^{\text{cur}} = \mathbf{K}^{-T}\mathbf{K}^{-1}$ by our assumption, we can express update of \mathbf{S}_K in terms of \mathbf{K} as follows.

$$\bar{\mathbf{S}}_K^{\text{new}} \leftarrow (1 - \beta_1)\bar{\mathbf{S}}_K^{\text{cur}} + \beta_1(\mathbf{U} + \lambda\mathbf{I}) = \mathbf{K}^{-T} \left(\mathbf{I} + \beta_1 \left(\mathbf{K}^\top \mathbf{U} \mathbf{K} + \lambda \mathbf{K}^\top \mathbf{K} - \mathbf{I} \right) \right) \mathbf{K}^{-1} = \mathbf{K}^{-T} (\mathbf{I} + \beta_1 \mathbf{m}_K) \mathbf{K}^{-1}$$

$\bar{\mathbf{S}}_K^{\text{new}}$ in the KFAC update can be approximated as below, where we consider $\mathbf{I} + \beta_1 \mathbf{m}_K$ as an approximate of the matrix exponential $\text{Exp}(\beta_1 \mathbf{m}_K) \approx \mathbf{I} + \beta_1 \mathbf{m}_K$ and notice that \mathbf{m}_K is symmetric.

$$\bar{\mathbf{S}}_K^{\text{new}} = \mathbf{K}^{-T} (\mathbf{I} + \beta_1 \mathbf{m}_K) \mathbf{K}^{-1} \approx \mathbf{K}^{-T} \text{Exp}(\beta_1 \mathbf{m}_K) \mathbf{K}^{-1} = \mathbf{K}^{-T} \text{Exp} \left(\frac{\beta_1}{2} \mathbf{m}_K \right)^\top \text{Exp} \left(\frac{\beta_1}{2} \mathbf{m}_K \right) \mathbf{K}^{-1}.$$

Informally, we can see that $\mathbf{K}^{\text{new}}(\mathbf{K}^{\text{new}})^\top$ approximates $(\bar{\mathbf{S}}_K^{\text{new}})^{-1}$ by using the matrix exponential. We can see that \mathbf{m}_K stays in a matrix logarithm space.

$$(\bar{\mathbf{S}}_K^{\text{new}})^{-1} \approx \mathbf{K} \text{Exp} \left(-\frac{\beta_1}{2} \mathbf{m}_K \right) \text{Exp} \left(-\frac{\beta_1}{2} \mathbf{m}_K \right)^\top \mathbf{K}^\top \approx \mathbf{K} \left(\mathbf{I} - \frac{\beta_1}{2} \mathbf{m}_K \right) \left(\mathbf{I} - \frac{\beta_1}{2} \mathbf{m}_K \right)^\top \mathbf{K}^\top = \mathbf{K}^{\text{new}}(\mathbf{K}^{\text{new}})^\top$$

Theorem 1 formally shows that $\mathbf{K}\mathbf{K}^\top$ used in our update is an approximation of $(\mathbf{S}_K + \lambda\mathbf{I})^{-1}$ in the KFAC update for every step even when the truncation of the matrix exponential is employed.

E PROOF OF THEOREM 1

We first consider the following lemmas in order to prove Theorem 1.

Recall that we denote $\bar{\mathbf{S}}_K := \mathbf{S}_K + \lambda\mathbf{I}$. For notation simplicity, we will drop the subscript K in this section and use $\bar{\mathbf{S}}_t$ to denote $\bar{\mathbf{S}}_K$ at iteration t . Notice that $\bar{\mathbf{S}}_t$ is non-singular at each iteration t so that we can inverse it in the original KFAC update (see Fig. 3).

Lemma 1 *Consider the following update in the original KFAC update at iteration t .*

$$\bar{\mathbf{S}}_t := (1 - \beta_1)\bar{\mathbf{S}}_{t-1} + \beta_1(\hat{\mathbf{U}}_{t-1} + \lambda\mathbf{I})$$

where \mathbf{S}_t is the factor \mathbf{S}_K used in the original KFAC update, β_1 is known as the weight of the moving average, and $\hat{\mathbf{U}}_{t-1}$ is a curvature matrix.

The initial factor $\bar{\mathbf{S}}_0$ can be decomposed as $\bar{\mathbf{S}}_0 = \hat{\mathbf{K}}_0^{-T} \hat{\mathbf{K}}_0^{-1}$ since $\bar{\mathbf{S}}_0$ as a preconditioning factor is symmetric positive definite.

Define $\hat{\mathbf{N}}_i := \hat{\mathbf{K}}_0^T \hat{\mathbf{U}}_i \hat{\mathbf{K}}_0 + \lambda \hat{\mathbf{K}}_0^T \hat{\mathbf{K}}_0 - \mathbf{I}$.

The Kronecker factor can be reexpressed as

$$\bar{\mathbf{S}}_t = \hat{\mathbf{K}}_0^{-T} \left(\mathbf{I} + \beta_1 \sum_{i=0}^{t-1} \hat{\mathbf{N}}_i \right) \hat{\mathbf{K}}_0^{-1} + O(\beta_1^2)$$

Lemma 2 Consider the following update in our inverse-free KFAC at iteration t .

$$\mathbf{K}_t := \mathbf{K}_{t-1} \left(\mathbf{I} - \frac{\beta_1}{2} \left(\mathbf{K}_{t-1}^\top \mathbf{U}_{t-1} \mathbf{K}_{t-1} + \lambda \mathbf{K}_{t-1}^\top \mathbf{K}_{t-1} - \mathbf{I} \right) \right)$$

where $\mathbf{K}_{t-1}^\top \mathbf{U}_{t-1} \mathbf{K}_{t-1}$ is used in our update and \mathbf{U}_{t-1} is a curvature matrix.

Define $\mathbf{N}_i := \mathbf{K}_i^\top \mathbf{U}_i \mathbf{K}_i + \lambda \mathbf{K}_i^\top \mathbf{K}_i - \mathbf{I}$.

Our update of \mathbf{K} can be reexpressed as

$$\mathbf{K}_t = \mathbf{K}_0 \left(\mathbf{I} - \frac{\beta_1}{2} \sum_{i=0}^{t-1} \mathbf{N}_i \right) + O(\beta_1^2)$$

Moreover, the product $\mathbf{K} \mathbf{K}^\top$ can be reexpressed as

$$\mathbf{K}_t \mathbf{K}_t^\top = \mathbf{K}_0 \left(\mathbf{I} - \beta_1 \sum_{i=0}^{t-1} \mathbf{N}_i \right) \mathbf{K}_0^\top + O(\beta_1^2)$$

Lemma 3 is useful to establish a relationship between the KFAC update and our inverse-free update.

Lemma 3 If we use the same sequence of curvature matrices in both the original KFAC update and our update such as $\hat{\mathbf{U}}_i = \mathbf{U}_i$ for each iteration i and $\hat{\mathbf{K}}_0 = \mathbf{K}_0$ are used on the initialization, we have the following expression.

$$\mathbf{N}_i = \hat{\mathbf{N}}_i + O(\beta_1)$$

Similarly, we have the following result for \mathbf{C} .

Theorem 2 The product $\mathbf{C} \mathbf{C}^\top$ has a first-order accuracy of the KFAC update of $(\mathbf{S}_C + \lambda \mathbf{I})^{-1}$ at each iteration if the update of \mathbf{C} is updated according to Figure 3 with the truncation of the matrix exponential and these two updates use the same initialization and the same sequence of curvature matrices \mathbf{G} .

$$\mathbf{C} \mathbf{C}^\top = (\mathbf{S}_C + \lambda \mathbf{I})^{-1} + O(\beta_1^2)$$

E.1 PROOF OF LEMMA 1

We prove the lemma by induction. We first show the base case when $t = 1$. By definition, we have

$$\bar{\mathbf{S}}_1 = (1 - \beta_1) \bar{\mathbf{S}}_0 + \beta_1 (\hat{\mathbf{U}}_0 + \lambda \mathbf{I}) \quad (11)$$

$$= (1 - \beta_1) \hat{\mathbf{K}}_0^{-T} \hat{\mathbf{K}}_0^{-1} + \beta_1 (\hat{\mathbf{U}}_0 + \lambda \mathbf{I}) \quad (12)$$

$$= \hat{\mathbf{K}}_0^{-T} \left[\mathbf{I} + \underbrace{\beta_1 \left(\hat{\mathbf{K}}_0^T \hat{\mathbf{U}}_0 \hat{\mathbf{K}}_0 + \lambda \hat{\mathbf{K}}_0^T \hat{\mathbf{K}}_0 - \mathbf{I} \right)}_{=\mathbf{N}_0} \right] \hat{\mathbf{K}}_0^{-1} \quad (13)$$

$$= \hat{\mathbf{K}}_0^{-T} \left[\mathbf{I} + \beta_1 \hat{\mathbf{N}}_0 \right] \hat{\mathbf{K}}_0^{-1} \quad (14)$$

Thus, the claim holds when $t = 1$.

Suppose, the claim holds when $t = n$. By the claim, we have

$$\bar{\mathbf{S}}_n = \hat{\mathbf{K}}_0^{-T} \left(\mathbf{I} + \beta_1 \sum_{i=0}^{n-1} \hat{\mathbf{N}}_i \right) \hat{\mathbf{K}}_0^{-1} + O(\beta_1^2) \quad (15)$$

Now, we consider the case when $t = n + 1$. Notice that

$$\begin{aligned}(1 - \beta_1)\bar{\mathbf{S}}_n &= \hat{\mathbf{K}}_0^{-T} \left(\mathbf{I} + \beta_1 \sum_{i=0}^{n-1} \hat{\mathbf{N}}_i - \beta_1 \mathbf{I} + O(\beta_1^2) \right) \hat{\mathbf{K}}_0^{-1} + O(\beta_1^2) \\ &= \hat{\mathbf{K}}_0^{-T} \left(\mathbf{I} + \beta_1 \sum_{i=0}^{n-1} \hat{\mathbf{N}}_i - \beta_1 \mathbf{I} \right) \hat{\mathbf{K}}_0^{-1} + O(\beta_1^2)\end{aligned}$$

By the definition of $\hat{\mathbf{S}}_{n+1}$, we have

$$\bar{\mathbf{S}}_{n+1} = (1 - \beta_1)\bar{\mathbf{S}}_n + \beta_1(\hat{\mathbf{U}}_n + \lambda \mathbf{I}) \quad (16)$$

$$= \hat{\mathbf{K}}_0^{-T} \left(\mathbf{I} + \beta_1 \sum_{i=0}^{n-1} \hat{\mathbf{N}}_i \underbrace{- \beta_1 \mathbf{I} + \beta_1 \hat{\mathbf{K}}_0^T \hat{\mathbf{U}}_n \hat{\mathbf{K}}_0 + \beta_1 \lambda \hat{\mathbf{K}}_0^T \hat{\mathbf{K}}_0}_{= \beta_1 \hat{\mathbf{N}}_n} \right) \hat{\mathbf{K}}_0^{-1} + O(\beta_1^2) \quad (17)$$

$$= \hat{\mathbf{K}}_0^{-T} \left(\mathbf{I} + \beta_1 \sum_{i=0}^n \hat{\mathbf{N}}_i \right) \hat{\mathbf{K}}_0^{-1} + O(\beta_1^2) \quad (18)$$

which is exactly the claim when $t = n + 1$.

Thus, by induction, the claim holds.

E.2 PROOF OF LEMMA 2

We prove the lemma by induction. We first show the base case when $t = 1$. By definition, we have

$$\mathbf{K}_1 = \mathbf{K}_0 \left(\mathbf{I} - \frac{\beta_1}{2} \underbrace{\left(\mathbf{K}_0^\top \mathbf{U}_0 \mathbf{K}_0 + \lambda \mathbf{K}_0^\top \mathbf{K}_0 - \mathbf{I} \right)}_{= \mathbf{N}_0} \right) \quad (19)$$

Thus, the claim holds when $t = 1$.

Suppose, the claim holds when $t = n$. By the claim, we have

$$\mathbf{K}_n = \mathbf{K}_0 \left(\mathbf{I} - \frac{\beta_1}{2} \sum_{i=0}^{n-1} \mathbf{N}_i \right) + O(\beta_1^2) \quad (20)$$

Now, we consider the case when $t = n + 1$. Notice that

$$\mathbf{K}_{n+1} = \mathbf{K}_n \left(\mathbf{I} - \frac{\beta_1}{2} \underbrace{\left(\mathbf{K}_n^\top \mathbf{U}_n \mathbf{K}_n + \lambda \mathbf{K}_n^\top \mathbf{K}_n - \mathbf{I} \right)}_{= \mathbf{N}_n} \right) \quad (21)$$

$$= \underbrace{\mathbf{K}_0 \left(\mathbf{I} - \frac{\beta_1}{2} \sum_{i=0}^{n-1} \mathbf{N}_i \right)}_{= \mathbf{K}_n - O(\beta_1^2)} \left(\mathbf{I} - \frac{\beta_1}{2} \mathbf{N}_n \right) + O(\beta_1^2) \quad (22)$$

$$= \mathbf{K}_0 \left(\mathbf{I} - \frac{\beta_1}{2} \sum_{i=0}^{n-1} \mathbf{N}_i - \frac{\beta_1}{2} \mathbf{N}_n + O(\beta_1^2) \right) + O(\beta_1^2) \quad (23)$$

$$= \mathbf{K}_0 \left(\mathbf{I} - \frac{\beta_1}{2} \sum_{i=0}^n \mathbf{N}_i \right) + O(\beta_1^2) \quad (24)$$

which is exactly the claim when $t = n + 1$.

Thus, by induction, the claim holds.

Notice that \mathbf{N}_i by definition is symmetric. It is easy to see that

$$\mathbf{K}_t \mathbf{K}_t^\top = \mathbf{K}_0 \left(\mathbf{I} - \frac{\beta_1}{2} \sum_{i=0}^{t-1} \mathbf{N}_i \right) \left(\mathbf{I} - \frac{\beta_1}{2} \sum_{i=0}^{t-1} \mathbf{N}_i \right)^\top \mathbf{K}_0^\top + O(\beta_1^2) \quad (25)$$

$$= \mathbf{K}_0 \left(\mathbf{I} - \frac{\beta_1}{2} \sum_{i=0}^{t-1} \mathbf{N}_i \right) \left(\mathbf{I} - \frac{\beta_1}{2} \sum_{i=0}^{t-1} \mathbf{N}_i \right) \mathbf{K}_0^\top + O(\beta_1^2) \quad (26)$$

$$= \mathbf{K}_0 \left(\mathbf{I} - \beta_1 \sum_{i=0}^{t-1} \mathbf{N}_i \right) \mathbf{K}_0^\top + O(\beta_1^2) \quad (27)$$

Thus, the claim also holds.

E.3 PROOF OF LEMMA 3

We first show the base case when $t = 1$. By the assumption, we have $\mathbf{K}_0 = \hat{\mathbf{K}}_0$. Similarly, we have $\mathbf{U}_0 = \hat{\mathbf{U}}_0$ by the assumption.

By definition, we have

$$\mathbf{N}_0 = \mathbf{K}_0^\top \mathbf{U}_0 \mathbf{K}_0 + \lambda \mathbf{K}_0^\top \mathbf{K}_0 - \mathbf{I} \quad (28)$$

$$= \hat{\mathbf{K}}_0^\top \hat{\mathbf{U}}_0 \hat{\mathbf{K}}_0 + \lambda \hat{\mathbf{K}}_0^\top \hat{\mathbf{K}}_0 - \mathbf{I} \quad (29)$$

$$= \hat{\mathbf{N}}_0 \quad (30)$$

Thus, the claim holds when $t = 0$.

When $t > 0$, we can use Lemma 2 to obtain the claim. Notice that

$$\mathbf{N}_{n+1} = \mathbf{K}_{n+1}^\top \mathbf{U}_{n+1} \mathbf{K}_{n+1} + \lambda \mathbf{K}_{n+1}^\top \mathbf{K}_{n+1} - \mathbf{I} \quad (31)$$

$$= \left(\mathbf{I} - \frac{\beta_1}{2} \sum_{i=0}^n \mathbf{N}_i \right)^\top \mathbf{K}_0^\top (\mathbf{U}_{n+1} + \lambda \mathbf{I}) \mathbf{K}_0 \left(\mathbf{I} - \frac{\beta_1}{2} \sum_{i=0}^n \mathbf{N}_i \right) - \mathbf{I} + O(\beta_1^2) \text{ (Lemma 2)} \quad (32)$$

$$= \mathbf{K}_0^\top (\mathbf{U}_{n+1} + \lambda \mathbf{I}) \mathbf{K}_0 + O(\beta_1) + O(\beta_1^2) \quad (33)$$

$$= \hat{\mathbf{K}}_0^\top (\hat{\mathbf{U}}_{n+1} + \lambda \mathbf{I}) \hat{\mathbf{K}}_0 + O(\beta_1) \quad (34)$$

$$= \hat{\mathbf{N}}_n + O(\beta_1) \quad (35)$$

E.4 PROOF OF THEOREM 1

It is sufficient to show that the following claim holds at iteration t since $\bar{\mathbf{S}}_t$ is non-singular.

$$\mathbf{K}_t \mathbf{K}_t^\top \bar{\mathbf{S}}_t = \mathbf{I} + O(\beta_1^2)$$

where we use $\bar{\mathbf{S}}_t$ to denote $\bar{\mathbf{S}}_K$ at iteration t .

By assumptions, we know that Lemmas 1, 2, 3 hold. Moreover, we have $\mathbf{K}_0 = \hat{\mathbf{K}}_0$. Thus, we have

$$\mathbf{K}_t \mathbf{K}_t^\top \bar{\mathbf{S}}_t = \mathbf{K}_0 \left(\mathbf{I} - \beta_1 \sum_{i=0}^{t-1} \mathbf{N}_i \right) \mathbf{K}_0^\top \bar{\mathbf{S}}_t + O(\beta_1^2) \text{ (by Lemma 2)} \quad (36)$$

$$= \mathbf{K}_0 \left(\mathbf{I} - \beta_1 \sum_{i=0}^{t-1} \mathbf{N}_i \right) \mathbf{K}_0^\top \hat{\mathbf{K}}_0^{-T} \left(\mathbf{I} + \beta_1 \sum_{i=0}^{t-1} \hat{\mathbf{N}}_i \right) \hat{\mathbf{K}}_0^{-1} + O(\beta_1^2) \text{ (by Lemma 1)} \quad (37)$$

$$= \hat{\mathbf{K}}_0 \left(\mathbf{I} - \beta_1 \sum_{i=0}^{t-1} \hat{\mathbf{N}}_i + O(\beta_1^2) \right) \left(\mathbf{I} + \beta_1 \sum_{i=0}^{t-1} \hat{\mathbf{N}}_i \right) \hat{\mathbf{K}}_0^{-1} + O(\beta_1^2) \text{ (by Lemma 3)} \quad (38)$$

$$= \hat{\mathbf{K}}_0 \mathbf{I} \hat{\mathbf{K}}_0^{-1} + O(\beta_1^2) \quad (39)$$

$$= \mathbf{I} + O(\beta_1^2) \quad (40)$$

F INVARIANCE OF INGD AND SINGD

INGD and SINGD are scale invariant to the choice of the Kronecker approximation while KFAC and IKFAC are not. Recall that we use the following Kronecker approximation to approximate the Hessian.

$$\mathbf{U} \otimes \mathbf{G} \approx \nabla_\mu^2 \ell(\boldsymbol{\mu})$$

However, such an approximation is not unique. We can consider an equivalent approximation such as

$$(\alpha \mathbf{U}) \otimes (\alpha^{-1} \mathbf{G}) \approx \nabla_\mu^2 \ell(\boldsymbol{\mu})$$

where $\alpha \neq 0$ can be any arbitrary non-zero scalar.

INGD is invariant since the update scheme involving the approximation is scale invariant: $\text{Tr}(\mathbf{H}_C) \mathbf{H}_K = \text{Tr}(\mathbf{C}^T \mathbf{G} \mathbf{C}) \mathbf{K}^T \mathbf{U} \mathbf{K} = \text{Tr}(\mathbf{C}^T (\alpha^{-1} \mathbf{G}) \mathbf{C}) \mathbf{K}^T (\alpha \mathbf{U}) \mathbf{K}$. The invariance is also preserved in SINGD since structures and their subspace projection maps are closed under scalar multiplications.

In contrast, the updates of KFAC and IKFAC are not scale invariant. As an example, we consider using curvature approximations \mathbf{U} and $(\alpha \mathbf{U})$ to update \mathbf{S}_K^{-1} in KFAC, and denote the updated \mathbf{S}_K^{-1} by $\hat{\mathbf{S}}_K^{-1}$ and $\bar{\mathbf{S}}_K^{-1}$, respectively. As shown below, we cannot recover $\hat{\mathbf{S}}_K^{-1}$ from $\bar{\mathbf{S}}_K^{-1}$ by scale transformations and thus, the KFAC update is not scale invariant.

$$\hat{\mathbf{S}}_K^{-1} = [(1 - \beta_1) \hat{\mathbf{S}}_K + \beta_1 \mathbf{U} + \lambda \mathbf{I}]^{-1} \neq [(1 - \beta_1) \bar{\mathbf{S}}_K + \beta_1 (\alpha \mathbf{U}) + \lambda \mathbf{I}]^{-1} = \bar{\mathbf{S}}_K^{-1}$$

An attempt to make the update of \mathbf{S}_K invariant is to set the damping weight to be $\alpha \lambda$. However, the update of \mathbf{S}_C requires us to set the damping weight to be $\alpha^{-1} \lambda$ as shown below. Thus, it is impossible to make KFAC invariant without introducing individual damping weights.

$$\hat{\mathbf{S}}_C^{-1} = [(1 - \beta_1) \hat{\mathbf{S}}_C + \beta_1 \mathbf{G} + \lambda \mathbf{I}]^{-1} \neq [(1 - \beta_1) \bar{\mathbf{S}}_C + \beta_1 (\alpha^{-1} \mathbf{G}) + \lambda \mathbf{I}]^{-1} = \bar{\mathbf{S}}_C^{-1}$$